

Archives of Toxicology

Toxic effects and biodistribution of ultrasmall gold nanoparticles

--Manuscript Draft--

Manuscript Number:	
Full Title:	Toxic effects and biodistribution of ultrasmall gold nanoparticles
Article Type:	Review
Corresponding Author:	Ulrich Simon, Prof. Dr. RWTH Aachen University Institute of Inorganic Chemistry Aachen, GERMANY
Corresponding Author Secondary Information:	
Corresponding Author's Institution:	RWTH Aachen University Institute of Inorganic Chemistry
Corresponding Author's Secondary Institution:	
First Author:	Ulrich Simon, Prof. Dr.
First Author Secondary Information:	
Order of Authors:	Ulrich Simon, Prof. Dr.
Order of Authors Secondary Information:	
Funding Information:	
Abstract:	<p>Abstract</p> <p>Gold nanoparticles (AuNPs) have been extensively explored in biomedical applications, for example as drug carriers, contrast agents, or therapeutics. However, AuNP can exhibit cytotoxic profile, when the size is below 2 nm (ultrasmall AuNP) and when the stabilizing ligands allow for access to the gold surface either for the direct interaction with biomolecules or for catalytic activity of the unshielded gold surface. Furthermore, ultrasmall AuNP exhibit significantly different biodistribution and enhanced circulation times compared to larger AuNP. By focusing on these findings this review acquaints the reader with the synthesis, the physico-chemical properties, the cytotoxicity studies as well as of the biodistribution and pharmacokinetics of ultrasmall AuNP.</p> <p>Keywords: gold nanoparticle, cytotoxicity, biodistribution, pharmacokinetics</p>
Suggested Reviewers:	

[Click here to view linked References](#)

Toxic effects and biodistribution of ultrasmall gold nanoparticles

Günter Schmid^{1*}, Wolfgang G. Kreyling², Ulrich Simon³

¹ Institute of Inorganic Chemistry, University Duisburg-Essen, Universitätsstr. 5-7, 45127 Essen, Germany

² Helmholtz Zentrum München - German Research Center for Environmental Health, Institute of Epidemiology 2, Ingolstaedter Landstrasse 1, 85764 Neuherberg / Munich, Germany

³ Institute of Inorganic Chemistry, RWTH Aachen University, Landoltweg 1a, 52074 Aachen, Germany

*: e-mail: Guenter.Schmid@uni-due.de

Abstract

Gold nanoparticles (AuNPs) have been extensively explored in biomedical applications, for example as drug carriers, contrast agents, or therapeutics. However, AuNP can exhibit cytotoxic profile, when the size is below 2 nm (ultrasmall AuNP) and when the stabilizing ligands allow for access to the gold surface either for the direct interaction with biomolecules or for catalytic activity of the unshielded gold surface. Furthermore, ultrasmall AuNP exhibit significantly different biodistribution and enhanced circulation times compared to larger AuNP. By focusing on these findings this review acquaints the reader with the synthesis, the physico-chemical properties, the cytotoxicity studies as well as of the biodistribution and pharmacokinetics of ultrasmall AuNP.

Keywords: gold nanoparticle, cytotoxicity, biodistribution, pharmacokinetics

1. Introduction

Gold in its macroscopic (bulk) state is known to be highly unreactive and is thus considered the noblest of all the metals (Hammer 2002). It is therefore the material of choice in various medical procedures, including reconstructive surgery, drug delivery microchips, endovascular stents, or as dental prostheses (Demann 2005) and is applied as a food additive and has the E number 175 (EFSA 2016). In its ionic state, as constituent of gold salts or molecular complexes, gold is a reactive metal, which, in turn, can also be utilized for therapeutic purposes, e.g. for the treatment of rheumatoid arthritis, where gold(I) thiolates are the principal compounds (Shaw 1999). Between the bulk and the molecular state, a new avenue is opened by nanometer sized gold particles (gold nanoparticles; AuNP), which exhibit physico-chemical properties, which may differ drastically from the bulk and molecular state and that are characterized by properties, that are determined by size as an independent parameter (Daniel 2004, Schmid 2005). AuNP are likewise easy to synthesize, they are tunable in size (they typically span a size range from 1nm – 100 nm in diameter) and shape, including spheres, rods, hollows spheres, cubes etc. (Grzelczak 2008). Besides the most striking feature, namely the increasing number of surface atoms with decreasing size as a general feature of nanoparticles, other properties are determined by the particles size, such as the melting point (Schmid 2003) or the electronic structure (Häkkinen 2008), which are invariant with size in the bulk state.

An optical property, that appears on the nanoscale, is the so-called surface plasmon resonance (SPR) (El-Sayed 2003), which will be explained briefly below. The spectral position of the SPR can be adjusted via size and shape of the AuNP, which has led to several new biomedical applications in diagnostics, such as bimolecular sensing (Schmid 2003). Meanwhile, therapeutic applications are being discussed in literature as well, which utilize the SPR e.g. for photoacoustic imaging (Li 2015) or NIR-responsive controlled release (Yavuz 2009).

The perspective to explore applications *in vivo* as well as the fact, that AuNP are increasingly applied in technical environments, for examples as catalysts (Tyo 2015) or as building blocks in nanoelectronic devices (Homburger 2009), concerns arise with respect to potential toxicities, as this may lead to unintended (and thereby uncontrolled) instead of intended (controlled) exposure. This has prompted numerous studies on the size dependent cytotoxicity of AuNP *in vitro* and *in vivo* (e.g. Alkilany 2010, Jia 2017, Soenen 2012) that covered the above mentioned size range below 100 nm and that included different surface ligands, that need to be applied to stabilize the particles in solution and to prevent them from agglomeration in biological media. Most of the toxicity studies considered AuNP, which are stabilized by organic molecules carrying thiol moieties, which allow for strong anchoring of the ligand to the AuNP's surface. Furthermore, the increasing use of AuNP in medical and technical fields lead to increasing exposure in many occupations but also of consumers and therefore the public at large and

1 patients being exposed with novel AuNP containing medication for diagnostics and therapy (Stone
2 2016). Exposures of consumers are dominated mainly via ingestion but also via inhalation, whereas
3 exposure of patients occurs via injections mostly intravenously and also via ingestions, depending on
4 the prescribed medications. Dermal exposures may occur, however, the existing evidence suggests
5 that intake through the skin is usually not detectable.
6
7

8
9 As a result of possible exposures the organs of intake are the respiratory tract, the digestive tract and
10 blood circulation. In recent years it became evident that not only the organs of intake will be exposed
11 but also secondary organs like liver, spleen, kidneys, heart, brain, the reproductive system, and also
12 tissues like those of the skeleton, the central nervous system and the immune-competent system.
13 Twenty years ago, particularly, the exposure of secondary organs and tissues was believed to be
14 negligible since the masses of nanoparticles, including AuNP, was so minute that any mass
15 concentration based adverse health effects in secondary organs were dismissed. Meanwhile
16 nanotoxicological research demonstrated that nanoparticles can pose risks according to their unique
17 physico-chemical properties such as their specific surface, area their very large number of individual
18 particles and their increased reactivity with biological fluids and tissues. In addition, cardio-vascular
19 effects observed in epidemiological studies triggered the discussion on enhanced translocation of
20 ultrafine particles from the respiratory epithelium towards the circulation and subsequent organs,
21 such as heart, liver, spleen and brain, eventually causing adverse effects on cardiac function and blood
22 coagulation, as well as on functions of the central nervous system. There is clear evidence that NP can
23 cross body membranes and reach the above mentioned secondary organs and accumulate there, as
24 most recently demonstrated by Miller et al., who showed that inhaled AuNP may accumulate at sites
25 of vascular disease (Miller 2017).
26
27
28
29
30
31
32
33
34
35
36
37
38
39

40 However, to this date, the understanding of the bioactivity and biodistribution of AuNP, taking in
41 account the particles size as a dominant parameter together with the composition (charge, polarity,
42 thickness etc.) of the ligand shell and its binding characteristics between gold surface and ligand
43 molecule, still requires well designed and interdisciplinary research and, eventually, re-evaluation of
44 the existing data. Thereby, apparent inconsistencies in toxicological evaluation, which arise from
45 different experimental conditions (cell lines, animal models, etc.), exposure times, doses and different
46 experimental methods to determine the distribution and fate of the applied AuNP, need to be clarified.
47 Hence, the present state of knowledge is sometimes characterized by conflicting conclusions, so that
48 toxicity issues either resulting from intended or unintended exposure, is still under debate (Khlebtsov
49 2011).
50
51
52
53
54
55
56
57

58 Irrespective of the lack of a systematic toxicological and pharmacokinetic classification of the
59 continuously increasing group and diversity of AuNP synthesized, it became evident, that in particular
60
61
62
63
64
65

1
2
3
4
5
6
7
8
9
10
11
12
13
14
15
16
17
18
19
20
21
22
23
24
25
26
27
28
29
30
31
32
33
34
35
36
37
38
39
40
41
42
43
44
45
46
47
48
49
50
51
52
53
54
55
56
57
58
59
60
61
62
63
64
65

ultrasmall AuNP in the size range below 2 nm can develop a toxic profile (Leifert 2013b). In this context, the size-dependent cytotoxicity of AuNP stabilized by sodium 3-(diphenylphosphino)benzene sulfonate (TPPMS) ligands was reported, whereby highest toxicity was observed for ultrasmall AuNP, having a core diameter of 1.4 nm (Au1.4MS). Smaller and larger TPPMS capped and glutathione (GSH) or thioglucose (e.g. used as ligand in the commercial product Aurovist) capped AuNP of similar size were much less toxic. In addition, in patch clamp experiments particularly Au1.4MS showed irreversible blocking of potassium ion channels (hERG channels), whereas thiol-stabilized AuNP of similar size did not.

A key to understand these unexpected findings is twofold: i) the extraordinary stability of the 1.4nm-sized gold core, which is obtained as a water-soluble derivative of the gold cluster $\text{Au}_{55}(\text{PPh}_3)_{12}\text{Cl}_6$ (Au_{55}). Au_{55} is a so-called full shell cluster, with a gold core consisting of 55 gold atoms, and exhibiting size-specific physico-chemical properties, including high catalytic activity in oxidation reactions with dioxygen (Turner 2008) and a discrete electronic structure that places the cluster in the intermediate state between a metal and a molecule (Schmid 2008). ii) the specific binding situation between AuNP and ligands. In general, AuNP need to be stabilized by ligands which have to be electron donors (Lewis base) binding coordinatively and via van der Waals forces to surface atoms of the NPs (Lewis acid) (Reimers 2017). The ligands may be carboxylic acids, amines, phosphines and thiols, whereas the ligand-to-metal binding strength follows the order $\text{O} < \text{N} < \text{P} < \text{S}$, according to Pearson's Hard and Soft Acids and Bases (HSAB) concept. The toxicity effect of the 1.4-nm-sized were abolished when the phosphine ligands were replaced by thiols having a stronger binding affinity to the gold surface and providing a more stable shielding of the gold core towards the biological environment.

This illustrates that AuNP can exhibit cytotoxic profile, when the size is below 2 nm and when the stabilizing ligands allows for direct access to the gold surface either for the direct interaction with biomolecules or for catalytic activity of the unshielded gold surface. As an additional size dependent feature, Au1.4MS showed in vivo experiments significantly different biodistribution, and enhanced circulation times compared to larger AuNP (Semmler 2008) While the larger particles accumulated in the liver, 1.4 nm AuNPs were detected in other organs as well, which is considered essential for any kind of therapeutic application of ultrasmall AuNPs (Hirn 2011).

By focusing on these findings this article gives an overview about the synthesis, the physico-chemical properties, the cytotoxicity studies as well as of the biodistribution and pharmacokinetics of ultrasmall AuNP, in particular of Au1.4MS as the key compound.

2. Synthesis of ultrasmall gold nanoparticles, in particular $\text{Au}_{55}(\text{PPh}_3)_{12}\text{Cl}_6$

2.1 Syntheses

The synthesis of $\text{Au}_{55}(\text{PPh}_3)_{12}\text{Cl}_6$, in the following called 1.4 nm AuNP, has been published the first time in 1981 (Schmid 1994, Schmid 2004). The transition from bulk gold to nanoparticles (earlier called colloids) is not only the reduction in size, but numerous other things change, for instance the melting point and the colour. As Figure 1 impressively shows, the transition from bulk gold to colloids is accompanied by the change of the well-known golden colour to ruby red. This effect, known since ancient years, is often used to colour glasses.

Fig. 1 The colour of metallic gold and gold nanoparticles in ruby glass. Reprinted from ref. Corain 2008 with permission from Elsevier Science.

The original synthesis of the 1.4 nm Au particle can be seen from Figure 2. It is performed from $(\text{PPh}_3)\text{AuCl}$ and B_2H_6 in toluene (Schmid 1981). Other substituents on the surface, necessary for protection and preventing coalescence, are monosulfonated phosphines, making the cluster water soluble, alternatively the SH-functionalized $(\text{cyclopentyl})_7\text{Si}_8\text{O}_{12}(\text{CH}_2)_3\text{SH}$ ($\text{T}_8\text{-OSS-SH}$), or the doubly charged $[\text{B}_{12}\text{H}_{11}\text{SH}]^{2-}$, all can be used to substitute PPh_3 and are shown in Figure 3 (Schmid 2008).

Fig.2 Synthesis of $\text{Au}_{55}(\text{PPh}_3)_{12}\text{Cl}_6$ from $(\text{PPh}_3)\text{AuCl}$ and B_2H_6

Fig. 3 Substitution of PPh_3 in $\text{Au}_{55}(\text{PPh}_3)_{12}\text{Cl}_6$, generating hydrophilic or hydrophobic character. Reprinted from ref. Schmid 2008 with permission from the Royal Society of Chemistry.

The reason for the phenomenon of colour change is best explained by the Mie theory (Mie 1908). It is based on the appearance of a plasmon resonance. This is strictly related to a distinct size of the corresponding metal. On the other hand, this is based on the presence of a confined electron gas interacting with light. A simplified explanation is shown in Figure 4.

1
2
3
4
5
6
7
8
9
10
11
12
13
14
15
Fig. 4 Illustration of the interaction of visible light and the confined electron gas of a metal nanoparticle, leading to a plasmon resonance, ruby red in case of gold. Reprinted from ref. Corain 2008 with permission from Elsevier.

16
17
18
19
20
21
22
23
24
25
26
27
28
29
30
31
32
33
34
35
36
37
38
39
40
41
42
43
44
45
46
47
48
49
50
51
52
53
54
55
56
57
58
59
60
61
62
63
64
65
Synthesis of the ruby red AuNPs, which are larger than the 1.4 nm Au₅₅ cluster, are available by chemical reduction of metal salts including electrochemical pathways (Fu 2002, Ohde 2002, Henglein 2000, Li 2000, Narayanan 2004, Crooks 2001) or thermolysis (Tano 1989, Esumi 1989, Esumi 1990, Esumi 1991, Esumi 1992b, Esumi 1992a).

Au₅₅(PPh₃)₁₂Cl₆ is, on the contrary to the larger Au NPs, not red, but brown, in solution, dependent on the concentration, yellowish. This is due to its molecular character. The Mie theory is no longer valid.

The 1.4 nm Au NP belongs to the so-called full-shell clusters of the general formula $10n^2 + 2$. n is the shell number. They consist either of cuboctahedral or icosahedral structure. Figure 5 shows the formation of cuboctahedrally structured full-shell clusters.

Fig 5 Stepwise formation of full-shell clusters 13 (1+12), 55 (13 + 42) 147 (55 + 92) and 309 (147 + 162). Reprinted from ref. Schmid 2008 with permission from the Royal Society of Chemistry.

The first metal atom can be coordinated by 12 equivalent atoms. Result: One-shell cluster consisting of 13 atoms. 13 atoms as a nucleus plus 42 additional Au atoms results in a two-shell cluster of 55 atoms. These clusters should be monodisperse, Of course it cannot be differentiated if there are 55, 54 or 56 atoms, but the monodispersity can be followed from TEM investigations. Figure 5a shows a TEM image of a single Au₅₅ cluster, Figure 6b a monolayer of Au₅₅ clusters with magnified cut-outs.

Fig 6 TEM Image of a Au₅₅ core (a) (reprinted with permission from ref. Schmid 1992. Copyright (1992) American Chemical Society) and a monolayer of Au₅₅ cores with magnified cutouts showing the monodispersity of the cluster (b) (reprinted with permission from ref. Schmid 2000 from John Wiley and Sons).

2.2 Electronic Properties

1
2 Why is the 1.4 nm Au cluster so special? The reason for their special behaviour is to be seen in their
3 electronic behaviour. It can be described as the transition between bulk and molecule. The stability of
4 the two-shell cluster $\text{Au}_{55}(\text{PPh}_3)_{12}\text{Cl}_6$ results from an impressive experiment. Surface deposited Au_{55}
5 clusters, separated from each other, and compared with smaller and larger Au clusters, are treated
6 with an oxygen plasma to remove the ligand shell. X-ray photoelectron spectroscopy (XPS) show
7 changes of all other particles, but not of Au_{55} (Boyen 2002). Figure 7 shows the results. Au_{55} only shows
8 a weak oxidic shoulder of a few clusters that are not exactly of full-shell type. All other species show
9 well-expressed signals for oxidic species. This method can therefore be used to cheque the purity of a
10 sample of $\text{Au}_{55}(\text{PPh}_3)_{12}\text{Cl}_6$.
11
12
13
14
15
16
17
18
19
20

21 **Fig 7** Au-4f photoelectron spectra of different Au nanoparticles, treated in an oxygen plasma. All except
22 Au_{55} show oxide signals. Reprinted from ref. Boyen 2002 with permission from The American
23 Association for the Advancement of Science.
24
25
26
27
28
29

30 Whereas in a bulk metal the electrons are distributed in so-called electronic bands. In small molecules
31 like $\text{Fe}_3(\text{CO})_{12}$ or $\text{Co}_4(\text{CO})_{12}$ the electrons are located in so-called molecular orbitals. The important
32 question is: where is the transition from bulk to molecule? Obviously, $\text{Au}_{55}(\text{PPh}_3)_{12}\text{Cl}_6$ performs all
33 necessary conditions at room temperature. At low temperatures larger particles also fulfil all the
34 conditions to serve as intermediates between bulk and molecule. Figures 8 and 9 show current (I)-
35 voltage (U) results that clearly show the situation.
36
37
38
39
40

41 Figure 8 shows the I-U behaviour of a 17 nm Pd particle at 295 K and at 4.2 K. At 295 it shows linear
42 metallic behaviour, following Ohm's law, whereas at 4.2 K there is a step, called Coulomb blockade.
43 (Bezryadin 1997).
44
45
46
47
48
49

50 **Fig 8** Current (I)-voltage (U) characteristics of a 17 nm Pd particle at 295 and 4.2 K. Reprinted from
51 Bezryadin 1997 with the permission of AIP Publishing.
52
53
54
55
56

57 Figure 9 proves that $\text{Au}_{55}(\text{PPh}_3)_{12}\text{Cl}_6$ already shows a Coulomb blockade at room temperature (Chi
58 1998).
59
60
61
62
63
64
65

1
2
3
4
5
6
7
8
9
10
11
12
13
14
15
16
17
18
19
20
21
22
23
24
25
26
27
28
29
30
31
32
33
34
35
36
37
38
39
40
41
42
43
44
45
46
47
48
49
50
51
52
53
54
55
56
57
58
59
60
61
62
63
64
65

Fig 9 I-U characteristic of $\text{Au}_{55}(\text{PPh}_3)_{12}\text{Cl}_6$ at room temperature indicating a well expressed Coulomb blockade. With kind permission from Springer Science+Business Media: Chi 1998.

The experimental setup to investigate such I-U characteristics is shown in Figure 10. It consists of a Scanning Tunneling Microscopy (STM) tip and a conductive surface. In between there is a single cluster molecule.

Fig 10 Experimental setup to image and to investigate ligand protected nanoparticles by STM and Scanning Electron Spectroscopy (STS), respectively. The conditions to observe single electron transitions are that $e^2/2C \gg k_B T$ where $C = \epsilon \epsilon_0 A/d$ is the capacity of the tunnel contact (ϵ_0 = electric field constant, A = surface of the electrode, d = distance of the electrodes). Adapted from ref. Schmid 2008 with permission from the Royal Society of Chemistry.

A STM image of $\text{Au}_{55}(\text{PPh}_3)_{12}\text{Cl}_6$ is shown in Figure 11 together with a model of the nanoparticle (Zhang 2003).

Fig 11 A: STM image of a single $\text{Au}_{55}(\text{PPh}_3)_{12}\text{Cl}_6$ cluster. The light green areas represent the electron rich phenyl rings of PPh_3 . The positions a and b have been used to measure STS spectra (Zhang 2003) (see Figure 12). B: Model of the cluster in the corresponding position. Reprinted from ref. Zhang 2003 with permission from American Chemical Society.

Fig 12 a: I-U characteristic of a single $\text{Au}_{55}(\text{PPh}_3)_{12}\text{Cl}_6$, measured at 7 K at two different positions. Reprinted from ref. Schmid 2008 with permission from the Royal Society of Chemistry. b: dI/dV characteristic of the curves a and b indicating discrete energy levels with spacing of 170 mV. Reprinted from ref. Zhang 2003 with permission from American Chemical Society.

Due to the low temperature, the Coulomb blockade is larger than at room temperature (see Figure 9). In Figure 12 the I-U characteristic is changed: the first ablation dI/dU is used instead of I and CB is indicated as a minimum. As can be seen from Figure 12 this minimum is characterized by a series of

1 energy levels with average spacings of 170 meV. In contrast to the bulk state, the energy bands have
2 disappeared.

3
4 Another method, characterizing the Au₅₅ core in Au₅₅(PPh₃)₁₂Cl₆, is to study the relaxation behaviour
5 of excited electrons and to compare it with other Au NPs (Smith 1997). Femtosecond laser
6 spectroscopy is the corresponding technique. The relaxation time depends on the electron-phonon
7 coupling and on the electron surface collision of electrons. Weakening of the electron-phonon coupling
8 dominates in large particles slowing down by electronic relaxation (see Fig 13, 15 nm particle). The 1.4
9 nm Au₅₅ nucleus is characterized by strong surface collisions, making relaxation faster. The reason for
10 the extremely slow relaxation behaviour of the 0.7 nm Au NP (Au₁₃) is that the electrons are strictly
11 located in the Au-Au bondings. The experimental result is shown in Figure 13 (Smith 1997).
12
13
14
15
16
17
18
19
20

21 **Fig 13** The relaxation behaviour of excited electrons of three Au NPs of different size. Reprinted from
22 Smith 1997 Copyright (1997), with permission from Elsevier.
23
24
25
26
27

28 These results prove impressively that Au₅₅ is just one step before the molecular state and differs
29 characteristically from the 15 nm Au NPs and especially from the bulk.
30

31
32 The last experimental study to prove the extraordinary position of the 1.4 nm Au₅₅(PPh₃)₁₂Cl₆ cluster
33 consists of EXAFS studies at 80 K. The results show that the bond lengths in the cluster are significantly
34 shorter than in bulk gold, indicating a cuboctahedral packing of the Au atoms. Comparable results
35 were obtained for the water soluble cluster Au₅₅(Ph₂PC₆H₄SO₃Na)₁₂Cl₆ (1993).
36
37
38
39

40 The conclusion of these experimental results finally is that Au₅₅(PPh₃)₁₂Cl₆ and its derivatives occupy a
41 very special position in gold cluster chemistry which will be supported by many other results, especially
42 in the field of cytotoxicity (see following chapters).
43
44
45

46 **3. Cytotoxicity and cellular uptake**

47
48 The first study on cytotoxic effects of Au1.4MS in a series of human cancer cell lines was reported in
49 2005 (Tsolis 2005). Eleven different cells lines were tested in comparison to Cisplatin (generic name
50 for the trade name drug Platinol® and Platinol®-AQ), which is an established anti-cancer
51 ("antineoplastic" or "cytotoxic") chemotherapy drug. These results are summarized in Table 1, which
52 informs on the IC₅₀ values of Cisplatin and Au1.4MS (here described as Au₅₅). In each case, Au1.4MS
53 turned out to be comparable or even more toxic than Cisplatin, especially considering the difference
54 in time to reach the respective IC₅₀ values, i.e. 24 h for Au1.4 MS and 72 h for Cisplatin.
55
56
57
58
59
60
61
62
63
64
65

1
2 **Table 1** IC₅₀ values of 11 human cancer cell lines treated with Cisplatin for 72 h and with Au_{1.4MS} (Au₅₅)
3 for 24 h. Table adapted from Tsoli 2005 with kind permission of John Wiley and Son.
4
5

6 These studies had been triggered by the previous findings that Au_{1.4MS} strongly interacts with B-DNA,
7 whereby it was observed that the ligand molecules, i.e. the weakly binding TPPMS ligands, are
8 substituted by DNA sections comprising the major grooves. This was explained by the specific size
9 conditions: the diameter of the cluster core is 1.4 nm and the height of the major groove in B-DNA is
10 1.3–1.5 nm. Supported by molecular calculations it was concluded that there are strong chemical
11 interactions between the Au₅₅ core and the DNA due to the polydentate character of the major grooves
12 (Liu 2003). Therefore, some of the phosphine ligands need to be removed from the original Au_{1.4MS},
13 so that Au₅₅ fits into the groove and thereby allows for interactions with electron-rich DNA
14 components, i.e. the phosphate groups of the DNA backbone. The coverage of B-DNA with Au₅₅
15 clusters has been visualized *ex vivo* by means of atomic force microscopy (AFM), after B-DNA was
16 incubated with Au_{1.4MS} in aqueous solution. Cross sections of the AFM image show the expected
17 difference in height between unloaded and cluster-containing DNA sections. The observed 1.8 nm
18 sections correspond with the sum of the DNA plus about half of the cluster, possibly still having some
19 ligand molecules outside. Figure 14a shows the AFM image and the cross section indicating the
20 difference between DNA with and without the 1.4-nm-sized AuNP, while Figure 14b depicts the result
21 of molecular modelling calculations, that propose the binding of the cluster into the major groove.
22
23
24
25
26
27
28
29
30
31
32
33
34
35
36
37

38 **Fig 14** (a) AFM image of DNA sections partially linked with Au₅₅ clusters. (b) Height profile of unloaded
39 and loaded parts, respectively. Figure reprinted with kind permission from Liu 2003 with kind
40 permission from John Wiley and Sons. c) Energy-minimized structure of B-DNA with Au₅₅ clusters along
41 the phosphate backbone of the major grooves. Figure reprinted from Tsoli 2005 with kind permission
42 from John Wiley and Sons.
43
44
45
46
47
48
49

50 These unexpected findings triggered a systematic study on the size dependent cytotoxicity ranging
51 from 0.8 nm to 15 nm with the cell lines HeLa, SK-Mel-28, L929, and J774A1 (Pan 2007). Tauredon, a
52 commercially available sodium aurothiamalate complex, being used for antirheumatic treatment, has
53 been applied as a reference. The results are illustrated in Figure 15.
54
55
56
57
58
59
60
61
62
63
64
65

1
2
3
4
5
6
7
8
9
10
11
12
13
14
15
16
17
18
19
20
21
22
23
24
25
26
27
28
29
30
31
32
33
34
35
36
37
38
39
40
41
42
43
44
45
46
47
48
49
50
51
52
53
54
55
56
57
58
59
60
61
62
63
64
65

Fig 15 Cytotoxicity of AuNP during the logarithmic growth phase of four cell lines. A) HeLa cells were seeded at 2000 cells/well and grown for 3 days into the logarithmic growth phase. AuNP were added for 48 h and MTT tests were performed. The logarithmic curve fits of tabulated MTT (3-(4,5-dimethylthiazol-2-yl)-2,5-diphenyltetrazolium bromide) readings are shown. Each data point represents the mean±standard error (SE) of sample triplicates. B) Note that the IC₅₀ values of Au1.4MS were lowest across all cell lines and that Au compounds of smaller or larger size were progressively less cytotoxic, which suggests a stringent size dependency of cytotoxicity. All concentrations relate to the amount of gold detected by atomic-absorption spectroscopy (AAS) in the authentic samples after performing the cytotoxicity test. This procedure ruled out the possibility that cluster synthesis contaminants or dilution errors may have caused erroneous results. Figure reprinted from Pan 2007 with kind permission from John Wiley and Sons.

In accordance to the previous findings, for the 1.4 nm AuNP IC₅₀ values ranging from 30 μM to 46 μM were obtained. Thence, this is the most toxic particle, as the IC₅₀ values of the particles with 0.8 nm (Au₉ cluster Gutrath 2013), 1.2 nm, and 1.8 nm were 250, 140, and 230 μM, respectively. These experiments also included reference measurements on pure ligands, as well as on a 1.4nm size AuNP with sodium 3,3',3''-triphenylphosphine sulfonate (TPPTS) as ligands, which is the threefold sulfonated derivative of triphenylphosphine, thus being higher negatively charged, as compared to the monosulfonated TPPMS. These particles (labeled as Au1.4TPPTS in Figure 16) showed similar IC₅₀ values as Au1.4MS. In contrast, the 15 nm AuNP were found to be non-toxic even at concentrations above 6.300 μM than the smaller particles, indicating a clear trend of decreasing cytotoxicity with increasing particle size. Another interesting outcome of this study was that also the cellular response is size dependent, in that 1.4-nm particles cause predominantly rapid cell death by necrosis within 12 h, while closely related AuNP with 1.2 nm in diameter effect predominantly programmed cell death by apoptosis.

These data were complemented in a very recent study, which analysed the cytotoxicity of AuNP in the size range between 1,4 nm and 15 nm, and thus fill the size gap between these two cornerstones of highest and lowest cytotoxicity (Broda 2016b). Besides Au1.4MS, AuNPs with 4.7nm, 10nm, 12nm, and 15nm, all stabilized with either TPPMS or TPPTS, respectively, were tested regarding their cytotoxicity towards HeLa cells. Again, Au1.4MS was found to be is the most cytotoxic species (IC₅₀ value of 43 μM), while all other particles showed decreasing toxicity with increasing size up to 15 nm, which corroborates the clear trend of size dependent toxicity. Furthermore, this studies disclosed that all TPPTS-stabilized AuNPs were found to be less toxic than TPPMS-stabilized ones.

1
2
3
4
5
6
7
8
9
10
11
12
13
14
15
16
17
18
19
20
21
22
23
24
25
26
27
28
29
30
31
32
33
34
35
36
37
38
39
40
41
42
43
44
45
46
47
48
49
50
51
52
53
54
55
56
57
58
59
60
61
62
63
64
65

Fig 16 IC₅₀ values of different sized TPPMS- and TPPTS-stabilized AuNPs achieved from citrate-stabilized AuNPs. IC₅₀ values are drawn in a logarithmic scale in given in μM Au. Therefore, a XTT (2,3-bis-(2-methoxy-4-nitro-5-sulfophenyl)-2H-tetrazolium-5-carboxanilide) vitality assay was applied by testing the cells during the logarithmic growth phase and determined the respective IC₅₀ values. Reprinted from Broda 2016b Copyright (2016), with permission from Elsevier.

Pan et al. pointed out that for Au1.4MS and Au15MS, the major cell-death pathway is oxidative stress (Pan 2009). All indicators of oxidative stress, reactive oxygen species (ROS), mitochondrial potential and integrity, and mitochondrial substrate reduction are compromised. In addition, they performed mRNA expression analysis using Affymetrix gene chips. The results are illustrated in Figure 17. In a so-called heat map presentation, it is illustrated that a group of growth-related genes (PTGER4, EDN1, NR4A1, C5orf13, NR4A3, EGR3, FOS, EMP1, CALD1, SERPINE1, EGR1, DUSP5, ATF3, DUSP2) were upregulated in HeLa cells treated with both Au1.4MS (the signature of these particles is “s”: small) and Au15MS (the signature of these particles is “b”: big) at 1 h after the onset of treatment (s1h_1, s1h_2, b1h_1, b1h_2). This reflected an initial growth response triggered by addition of fresh media along with the Au1.4MS and Au15MS, which illustrates a well-known short-term phenomenon of cell culture and confirms the validity of the gene chip expression study. A separate clustering of the gene expression changes following treatment with the non-toxic Au15MS confirmed an overlapping, almost identical group of genes (EGR1, NR4A1, DUSP5, PPP1R3B, EDN1, FOS, EGR1, EDN1, ADAMTS1, ATF3, PTGER4, CYR61) as upregulated at 1 h after medium exchange irrespective of toxicity. Following the initial growth response, heat shock and stress-related genes were upregulated after 6 h and strongly upregulated after 12 h in Au1.4MS-treated but not in Au15MS-treated or untreated HeLa cells. This group of genes (HSPA1A, DNAJA4, CHAC1, HSPA1A, DDIT3, GEM, LOC387763, PGF, HSPA6, SESN2, LOC284561, PPP1R15A, HMOX1, C16orf81, LOC344887, NGF, OSGIN1, FOSL1, CXCL2, IL8) suggested that a robust stress response had occurred in the Au1.4MS-treated cells. Highly elevated expression of heat shock proteins has been demonstrated to inhibit apoptosis at several stages including blocking of cytochrome c release from mitochondria, thus preventing the formation of an apoptosome and the activation of caspase-3, ultimately forcing cells into necrosis instead of apoptosis.

Fig 17 Hierarchical cluster analysis and heat-map representation of differentially regulated genes in AuNP-treated HeLa cells. All gene chip analyses were performed in duplicate (_1,_2). HeLa cells were left untreated (c) or were treated for 1, 6, and 12 h with Au1.4MS (s1h – s12h for small AuNPs) or with Au15MS (b1h – b12h for big AuNPs). Gene expression levels determined by Affymetrix gene chips were subjected to hierarchical cluster analysis. Upon treatment with Au1.4MS, 35 genes were significantly upregulated. Each gene is depicted by a single row of colored boxes. The color of the respective box in

1 one row represents the expression value of the gene transcript in one sample compared with the
2 median expression level of the gene's transcript for all samples shown. Blue, transcript levels below
3 median; white, transcript levels equal to median; red, transcript levels higher than median. Figure
4 reprinted from Pan 2009 with kind permission from John Wiley and Sons.
5
6

7 The gene expression profile in Au1.4MS is fully compatible with an oxidative stress response leading
8 to necrosis. The previous studies of AuNP interaction with DNA suggested that the toxicity of Au1.4MS
9 might be due to interference with DNA transcription. However, the strongly enhanced expression of
10 35 genes after exposure of HeLa cells to Au1.4MS and the continued expression of GAPDH both argued
11 against direct transcriptional inhibition by Au1.4MS. This indicates that binding of the metal core of
12 the Au1.4MS cannot be the sole or predominant reason for cytotoxicity. Nevertheless, a partial loss of
13 the ligand shell being essential for the DNA binding, is still considered as a precondition to unfold high
14 AuNP cytotoxicity. This is confirmed by different experimental approaches:
15
16

17 The first one analyses the effect of different reducing agents (RA) or antioxidants, i.e. N-acetylcysteine
18 (NAC), glutathione (GSH), ascorbic acid (ASC) and TPPMS, comprising different binding affinities to the
19 gold surface. The results are illustrated in Figure 18. If the cells are pre-treated for 3h with the
20 respective RA, washed and post-treated with Au1.4MS, the cytotoxicity is unaffected. If either
21 Au1.4MS was pre-treated with RA for 3 h and the mixture was added to the cells for 48 h, the cells
22 were pre-treated with RA for 3 h, followed by the addition Au1.4MS and incubated for 48 h, or the RA
23 was mixed with Au1.4MS and the mixture was immediately added to cells and incubated for 48 h,
24 toxicity of Au1.4MS was significantly reduced, except for ascorbic acid. This led to the conclusion that
25 the thiol-bearing molecules NAC and GSH as well as an excess of TPPMS stabilize the particles in
26 solution, so that the unshielding of the bare gold core due to a partial loss of the ligand shell, which
27 was anticipated as the precondition to unfold cytotoxicity, is prevented by the replacement of TPPMS
28 with NAC or GSH or is effectively reduced by an excess of free TPPMS via the chemical equilibrium.
29 This hypothesis was further confirmed by analysing AuNPs of similar size (1.1nm), that were directly
30 capped with glutathione (Au1.1GSH) (Pan 2009). These particles do not induce oxidative stress and
31 thus are almost non-toxic.
32
33
34
35
36
37
38
39
40
41
42
43
44
45
46
47
48
49
50
51

52 **Fig 18** Bar chart and the corresponding molecular structures of RA rested. NAC, GSH, and TPPMS but
53 not ascorbic acid can partially inhibit the cytotoxicity of 100mM Au1.4MS. A) Untreated cells. B) Cells
54 treated with Au1.4MS for 48 h. C) Cells pre-treated with reducing agent for 3 h, washed, and post-
55 treated with Au1.4MS for 48 h. D) Au1.4MS pre-treated with reducing agent for 3 h, and mixture added
56 to cells for 48 h. E) Cells pre-treated with reducing agent for 3 h, then Au1.4MS added and incubated
57
58
59
60
61

1
2
3
4
5
6
7
8
9
10
11
12
13
14
15
16
17
18
19
20
21
22
23
24
25
26
27
28
29
30
31
32
33
34
35
36
37
38
39
40
41
42
43
44
45
46
47
48
49
50
51
52
53
54
55
56
57
58
59
60
61
62
63
64
65

for 48 h. F) Reducing agent mixed with Au1.4MS and mixture immediately added to cells and incubated for 48 h. G) Cells incubated with reducing agent for 48 h. Figure reprinted from Pan 2009 with kind permission from John Wiley and Sons.

The second approach utilized patch clamp measurements as a Food and Drug Administration (FDA)-established drug safety test (FDA 2005). Depending on the ligand composition, the 1.4-nm-diameter AuNP failed electrophysiology-based safety testing using human embryonic kidney cell line 293 cells expressing human ether-á-go-go-Related gene (hERG) (Leifert 2013a). While the TPPMS-stabilized AuNP irreversibly blocked hERG channels, GSH-stabilized AuNPs of similar size had no effect *in vitro*, and neither particle blocked the channel *in vivo*, which also holds the addition of excess TPPMS (see Figure 19). The blockade of the hERG channel by Au1.4MS was irreversible and control experiments confirmed that it is not caused by the ligand TPPMS, which exhibited a reversible blockade, and only at very high concentrations. This confirms that the binding modality between metal and ligand is a relevant parameter, hence the shielding of the AuNP surface plays a crucial role in the cytotoxicity of Au1.4MS. These finding where supported by docking simulation of AuNPs, carrying a varying number of ligands in contact with the hERG channel, suggesting a differential interaction facilitated by the complementarity in size and shape.

Fig 19 Patch-clamp measurement of hERG tail current peak amplitudes in HEK 293 cells stably expressing the hERG ion channel. (a) Concentration-dependent inhibition of hERG current by Au1.4MS (3.1 μ M, 6.5 μ M, and 16.25 μ M gold atom concentrations), sequentially applied to the same cell. The shaded areas indicate the intervals of different compound concentrations [Au] and [TPPMS], respectively. After a latency time of typically 2–3 min, an increase in the slope of current decay with increasing Au1.4MS concentration is observed. Arrows indicate start (S), change (C), and end (E) of perfusion with the differently concentrated AuNP solutions. (b) Inhibition of hERG current by 65 μ MAu1.4MS shows no recovery upon washout. Arrows indicate start (S) and end (E) of perfusion with AuNP solution. The blocking of the hERG channel by Au1.4MS is irreversible and additive. (c) Application of 300 μ MAu1.1GSH did not affect the hERG current. The shaded areas indicate the intervals of different compound concentrations of [Au] in Au1.1GSH. (d) Preincubation of Au1.4MS with different concentrations of TPPMS abolished the hERG blocking potency of 20 μ MAu1.4MS when TPPMS was present in excess. The cell was perfused with a mixture of 20 μ MAu1.4MS +50 μ M TPPMS, 20 μ M Au1.4MS + 25 μ M TPPMS, and 20 μ M Au1.4MS + 10 μ M TPPMS. Reprinted from Leifert 2013 with kind permission of PNAS.

4. Cellular uptake and distribution

As pointed out before, the physico-chemical properties of inorganic nanoparticles, in general, depend on the intrinsic properties of the particle core as well as on the composition of the ligand shell (Draeden 2012). These ligands have several functions. Most important, they increase the colloidal stability of the particles in biological environments by steric or electrostatic means. Furthermore they are thought to enhance the biocompatibility of the inorganic NPs. Hence, the short- and long-term stability of the ligand shell is of vital importance for the evaluation of the bioactivity and fate of the particles *in vivo*. This does not only hold for weakly binding ligands, such as phosphines on gold. A recent study has demonstrated that even firmly grafted polymer shells around 5 nm AuNPs, bound to the gold core via thiol terminated, strongly binding anchor groups, may degrade within 24 h when injected into rats (Kreyling 2015). The findings discussed above indicate the need of detailed investigations on the intracellular integrity of the cytotoxic 1.4-nm-sized AuNP. Although, it is most likely that nanoparticle toxicity follows endocytosis, it is entirely possible that the toxicity may stem from interactions at the cell membrane, even though the particles are also endocytosed (Broda 2016a). However, the specific binding situation of the ligand shell in Au1.4MS may also promote direct penetration of the cell membrane, which is consistent with recent studies on the interaction of Au1.4MS with model membranes (Broda 2016b).

The localization of inorganic NP in cells can be analysed by means of transmission electron microscopy. However, imaging of inorganic NP, in particular in the sub-2nm range, is still a big technical challenge due to resolution limitations on biological media, caused e.g. by inelastic scattering or high electron beam sensitivity of the biological material (He 2007, Marquis 2009, Sousa 2012). Alternatively, AuNP in this size range can be traced in biological samples by using either nuclear radiation detection or fluorescence detection (for the ligand shell, if equipped with a fluorescence marker).

For nuclear radiation detection the isotope ^{197}Au , which is both a mononuclidic and monoisotopic element, is transferred into the radioactive isotope ^{198}Au by means of neutron activation ($^{197}\text{Au} (n, \gamma) ^{198}\text{Au}$), which allows for quantitative detection of Au in the biological samples. This analytical method is called neutron activation analysis, NAA. However, NAA is rather limited in spatial resolution so that quantification of gold is not feasible on a single cell level but requires integration over a larger number of cells. In contrast, ligand shell of AuNPs may directly be traced on the cellular level by utilizing fluorescence quenching (Ke 2014) and/or enhancing effects (Chowdhury 2006). In order to investigate the hypothesized ligand loss of Au1.4MS upon cellular uptake, new phosphine stabilized cytotoxic

1 Au1.4MS have been synthesized bearing a fluorophore, so that fluorescence de-quenching can be
2 utilized to visualize the fate of the ligand.

3
4 Broda et al. introduced a new type of cytotoxic 1.4-nm-sized AuNP, where the gold core is
5 functionalized with a fluorophore Cascade Blue Ethylenediamine[®] (CBE), described as Au1.4MS/CBE
6 (Broda 2016a). Upon binding of the fluorophore covalently to the AuNP-surface, the fluorescence
7 emission of the CBE is quenched. However, fluorescence reappears as soon as it is released from the
8 AuNP-surface (cf. Figure 20).
9
10
11
12
13
14

15 **Fig 20** (left) Cytotoxic 1.4-nm-sized AuNP are functionalized with a fluorophore Cascade Blue
16 Ethylenediamine[®]. In this state the fluorescence emission of the CBE is quenched. By ligand release
17 upon cellular uptake, fluorescence reappears and gets visible in the fluorescence images of HepG2 cells
18 (see Figure 21)). Figure reprinted from Broda 2016a with kind permission from John Wiley and Sons.
19
20
21
22
23
24
25

26 In order investigate the subcellular distribution of CBE, HepG2 cells we treated with 100 μ M of
27 Au1.4MS/CBE. Although cytotoxic effects have been observed, in cells with overall healthy morphology
28 CBE-molecules were found to be homogenously distributed over the cytoplasm and concentrated to
29 some extent at the cell membrane (Figure 21 a). Moreover, fluorescence was found inside the nucleus,
30 however, with lower intensity compared to the cytosol. The authors concluded that at least a fraction
31 of CBE is no longer covalently attached to the AuNP-surface (Broda 2016a). The released CBE was
32 furthermore able to enter the cell as well as the nucleus and could be found in various subcellular
33 compartments including cytosol, nucleus and plasma membrane. However, from the localization of
34 released fluorophores alone, it could neither be concluded where the detachment occurred nor could
35 be deduced that Au1.4MS/CBE has been taken up by the cells. In order to prove the uptake Au1.4MS,
36 irrespective of whether still bound to CBE or not, NAA on cell fractionations were carried out after
37 exposure of HepG2 cells to AuNPs.
38
39
40
41
42
43
44
45
46
47
48
49

50 **Fig 21** a) CLSM images of HepG2 cells incubated for 20 h with 100 μ M Au1.4MS/CBE or 100 μ M
51 Au1.4MS as indicated. Fluorescence (left) and bright-field images (right) are shown. Arrows point to
52 increased fluorescence at the cell membrane. Nuclei appear with lower fluorescence as exemplified
53 with dotted circles. Scale bars represent 10 μ m. b, c) Gold amounts determined via NAA for (b) cytosolic
54 and nuclear fractions and (c) for membrane and soluble fractions. HepG2 cells were incubated for 24
55 h with 1 and 75 μ M Au1.4MS or Au1.4MS/CBE. Figure reprinted from Broda 2016a with kind permission
56 from John Wiley and Sons.
57
58
59
60
61
62
63
64
65

1
2
3
4
5
6
7
8
9
10
11
12
13
14
15
16
17
18
19
20
21
22
23
24
25
26
27
28
29
30
31
32
33
34
35
36
37
38
39
40
41
42
43
44
45
46
47
48
49
50
51
52
53
54
55
56
57
58
59
60
61
62
63
64
65

In cells which were incubated with 75 μ M AuNP-solutions of Au1.4MS and Au1.4MS/CBE, respectively, (339 \pm 20) ng Au stemming from Au1.4MS and (569 \pm 113) ng Au stemming from Au1.4MS/CBE were found in the cytosolic fractions (Figure 21b). In contrast to previous studies (Verma 2010) only low amounts of gold were found in the nuclear fractions. The distribution of the incorporated AuNPs in the cytosolic and nuclear fraction is 96.6 to 3.4 % and 95.2 to 4.8 % for Au1.4MS and Au1.4MS/CBE, respectively. The differentiation between membrane-bound and incorporated AuNPs revealed membrane association of a substantial portion of both Au1.4MS and Au1.4MS/CBE (Figure 21 c). This is a priori surprising, as the particles are negatively charged and are thus not expected to be attached to the negatively charge cell membrane. However, membrane-bound negatively charge AuNPs may be bound non-specifically to cationic patches on the otherwise negatively charged membrane (Schaeublin 2011). The difference in overall lower gold amount detected is attributed to different procedure in cell fractionation.

The cellular uptake efficiency was derived from the sum of the detected gold amount in the soluble and the membrane fractions related to the applied gold amount. In accordance to previously reported data (Soenen 2012, Alkilany 2010), the cellular uptake efficiency is 2 – 3 %, which corresponds to approx.. 105 - 107 particles per cell (see Table 2). A generally higher uptake is reported for positively charged AuNPs (Alkilany 2010, Bogart 2014).

Table 2 Internalized AuNPs per cell and cellular uptake efficiencies of HepG2 cells incubated 24 h with 1 and 75 μ M Au1.4MS or Au1.4MS/CBE determined by referring the applied gold concentration to the sum of the gold amount found in the soluble and the membrane fractions Table reprinted from Broda 2016a with kind permission from John Wiley and Sons.

The data show that Au1.4MS/CBE was more efficiently taken up than Au1.4MS, although they exhibit a higher negative surface charge due to the three sulfonate groups per CBE group. The authors point out, that this is in line with the previously reported increased internalization of 1.5-nm-sized negatively charged AuNPs into HaCaT cells compared to cationic and neutral ones (Soenen 2012). This is attributed to the adsorption of serum proteins from the cell culture media, which could induce the entry of AuNPs into cells by receptor-mediated endocytosis (Rivera-Gil 2013, Rosi 2006). However, even if serum proteins are adsorbed onto the AuNPs' surface the effect on the cytotoxic properties is negligible as both particle species exhibit similar IC₅₀-values. This confirms the hypothesis that the partial or complete loss of the TPPMS ligand shell, to which serum proteins will bind, is a prerequisite to unfold the cytotoxicity of these ultras-small AuNP.

5. In vivo toxicity tested in zebrafish embryo essays

As pointed out in many works, the zebrafish embryo tests (FET) are considered suited as a complex vertebrate test to study the toxicity of nanoparticles (Scholz 2008, Kosmehl 2012). 25% of the zebrafish genes are known to be essential for early development and 99% of these genes are homologous to human genes (Amsterdam 2004). This suggest that results obtained in zebrafish may be transferable to humans. Anyway, they are highly useful for 'intermediate' toxicity testing, after completing initial experiments in cells, and before turning to in vivo experiments in rodents (Rizzo 2013).

Jahnen-Dechent and coworkers showed recently showed that FET reproduced all important findings of a previous study in HeLa cells concerning the toxicity effects of Au1.4MS, as discussed above, and added new important information on teratogenicity and hepatotoxicity that could not be gained from studying cultured cells (Pan 2013). They compared Au1.4MS and equally sized Au1.4GSH. In their study Au1.4MS caused embryo coagulation at the lethal dose of 400 mM. At a sub-lethal dose of 50 mM, Au1.4MS caused hypopigmentation and pericardial edema. The malformations were absent in embryos exposed to Au1.4GSH at an even higher dose (1 mM), and, in accordance to the cytotoxicity test in HeLa cells, the toxicity of Au1.4MS was drastically reduced, GSH when was added.

6. Antibacterial effects

In order to explore potential therapeutic activity of cytotoxic ultrasmall AuNP, Boda et al. investigated treatment option against staphylococcal infections (Boda 2015). The emergence of multidrug resistant bacteria, especially biofilm-associated Staphylococci, requires novel antimicrobial agents. The authors tested antibacterial activity of AuNPs in a size range between 0.8nm and 10 nm against planktonic gram-positive and gram-negative pathogenic bacteria. Among the grampositive strains, Staphylococcus aureus and S. epidermidis were tested, while Escherichia coli and Pseudomonas aeruginosa comprised the gram-negative strains. In concentration-dependent toxicity assessment, the minimum inhibitory concentration (MIC) and minimum bactericidal concentration (MBC) were evaluated. The results are summarized in Table 3.

Table 3 Summary of (A) MIC and (B) MBC of TPPMS-stabilized AuNP against different bacterial strains

They found that ultrasmall AuNPs with core diameters of 0.8 and 1.4 nm, i.e. Au0.8MS and Au1.4MS, both being stabilized with TPPMS, both have minimum inhibitory concentration (MIC) and minimum

1 bactericidal concentration of 25×10^{-6} M [Au]. However, in contrast to the previously discussed
2 cytotoxicity data, the bactericidal activity of Au0.8MS was found to be higher than for Au1.4MS. In
3 accordance to all previous findings, thiolstabilized AuNP (in this study, AuNP with diameter of 1.9 nm
4 (AuroVist) were used) did not cause significant toxicity in any of the bacterial strains.
5
6

7 In kill kinetics studies, were Au0.8MS and Au1.4 MS were studied at their MIC in staphylococci, both
8 particles caused acute toxicity in *S. aureus* and *S. epidermidis*, respectively. Thereby, an up to $5 \log_{10}$
9 reduction in viable bacteria was measured within 5 h of exposure. As can be seen in Figure 22, between
10 5 and 21 h, bacterial growth resumed due to the growth of resistant bacteria with the exception of
11 Au0.8MS treated *S. aureus*. This specific test did not show signs of recovery even after 24 h of culture.
12
13
14
15
16
17

18
19 **Fig 22** Growth kinetics of A) *S. aureus* and B) *S. epidermidis* exposed to Au0.8MS and Au1.4MS at MIC
20 (25×10^{-6} M Au) for 0–24 h, presented by the number of colony forming units per mL (cfu/mL). Figure
21 reprinted from Broda 2015 with kind permission from John Wiley and Sons.
22
23
24

25 Although, not explanation of the superior antibacterial properties of Au0.8MS is not explained, yet,
26 the results document antibacterial effects of ultras-small, TPPMS-stabilized AuNP below the IC 50
27 concentrations reported for eukaryotic cells. This suggests a therapeutic window for such particles
28 below host toxic concentrations.
29
30
31

32 33 34 35 36 **7. Biodistribution and pharmacokinetics**

37 To determine accumulated fractions in secondary organs and tissues the ultimate aim is to
38 quantitatively balance the fractions of NP in all relevant organs and tissues of the body and include the
39 remaining body and total excretion collected between application and analysis as a function of
40 retention time; i.e. quantitatively balanced biokinetics of the incorporated AuNP as described earlier
41 (Kreyling 2013, Geiser 2010). Note, selective analyses of selected organs may cause substantial
42 uncertainty of the fate of incorporated AuNP.
43
44
45
46
47
48
49
50

51 **7.2 Size dependent biokinetics after three routes of application**

52 For a systematic attempt of the effect of the AuNP size we used a suite of monodisperse AuNP ranging
53 from 1.4nm, 5nm, 18nm, 80nm and 200nm all surface-modified with TPPMS resulting in a negative
54 zeta-potential and, additionally, 2.8nm AuNP either coated with thioglycolic acid (TGA) exhibiting a
55 terminal carboxyl group (COO⁻) or with cysteamine group exhibiting a terminal amino group (NH₃⁺)
56 achieving either a negative or a positive zeta-potential. These AuNP were applied to healthy, adult
57
58
59
60
61
62
63
64
65

1 female rats via three routes (intratracheal (IT) instillation, oral ingestion by gavage and intravenous
2 tail-vein (IV) injection) to directly compare the effect caused by different organs of intake – lungs versus
3 gastro-intestinal-tract (GIT) versus systemic circulation in blood (Kreyling 2014, Schleh 2012, Hirn 2011,
4 Semmler-Behnke 2008).
5

6 All AuNP were radioactively labeled by neutron irradiation in a nuclear research reactor (^{197}Au (n, γ)
7 ^{198}Au) prior to use as described previously (Kreyling 2014, Schleh 2012, Hirn 2011, Semmler-Behnke
8 2008). Physicochemical parameters of the AuNP including specific ^{198}Au radioactivity and the isotope
9 ratio of ^{198}Au to stable ^{197}Au are given in the previous reports. Due to the short radioactive half-life of
10 ^{198}Au (2.7 d), biodistributions were quantitatively determined up to three times within the first 24
11 hours after application.
12

13 Figure 23 shows IT-instilled AuNP were retained predominantly in the lungs including small but size
14 dependent AuNP translocations towards blood circulation and subsequent accumulation in all
15 secondary organs and tissues (left panel); in contrast, more than 95% of the gavaged AuNP were
16 passing through the GIT for fecal excretion including even smaller but also size dependent fractions of
17 absorbed AuNP through the GIT-epithelia towards blood circulation and subsequent accumulation in
18 secondary organs and tissues (middle panel). In further contrast, after IV-injection AuNP were rapidly
19 cleared from circulation within one hour in a size dependent manner and predominantly accumulated
20 in liver (right panel) followed by spleen and other secondary organs as well as tissues (Figure 24).
21
22
23
24
25
26
27
28
29
30
31

32 **Fig 23** Size dependent 24-hour retentions AuNP in organs of intake (i.e. lungs, GIT, blood) as percentage
33 of initially applied dose (ID) after all three AuNP applications. In addition, total translocation across the
34 ABB and absorption across the GIT epithelium are shown after IT-instillation and gavage, respectively;
35 and the dominant liver accumulation after IV-injection (Kreyling 2014, Schleh 2012, Hirn 2011,
36 Semmler-Behnke 2008). Mean data \pm SEM of $n=4$ rats for each AuNP size. Note that the AuNP tested
37 are TPPMS stabilized except the 2.8nm AuNP, which are stabilized with thioglycolic acid (TGA)
38 exhibiting a terminal carboxyl group (COO^-).
39
40
41
42
43
44
45
46
47
48

49 Figure 24 compares the accumulation of 18 nm AuNP between 1-hour and 24-hours in secondary
50 organs and tissues after all three applications – IT-instillation, Gavage and IV-injection. In order to
51 compare accumulation in secondary organs and tissues directly between the three application routes,
52 fractions of the initially applied dose (ID) after IV-injection are compared with fractions relative to the
53 amount of AuNP which had entered blood circulation for subsequent accumulation after crossing the
54 ABB or the GIT-epithelium, respectively. It is remarkable how rapid accumulation had occurred already
55 one hour after application; further accumulation until 24-hours is rather modest in all secondary
56
57
58
59
60
61
62
63
64
65

1 organs and the remaining carcass after IT-instillation or IV-injection, respectively. However, after
2 gavage AuNP accumulation increases more than tenfold in spleen, kidneys, brain and carcass while in
3 liver the AuNP content declines an order of magnitude after one hour. In blood freshly IV-injected
4 AuNP decreased a thousand-fold within one hour and stayed constant at this low level during the next
5 24 hours. Neither the clearance mechanisms are fully understood but it appears that liver
6 macrophages (Kupffer cells) effectively and rapidly catch more than 90% of the circulating AuNP after
7 IV-injection while only about 1% AuNP are retained in both spleen and carcass and even lower fractions
8 are found in other organs. In contrast, of those AuNP which had crossed the ABB after IT-instillation,
9 the blood fraction is higher than 10% at one hour and declines gradually. AuNP fractions of about 10%
10 in the liver are as high as in blood and increase slightly over time. A similar gradual increase is seen in
11 the other secondary organs although on a lower level. Note, the highest content of translocated AuNP
12 (> 80%) is found in the carcass comprising of the skeleton, muscles, fat, skin, etc.

21 After gavage AuNP patterns are again different to those after IV-injection or IT-instillation; of those
22 AuNP which had crossed the GIT-epithelium, the AuNP fraction in blood is only 0.1% but increases
23 drastically a hundred-fold during the next 24 hours. Since in most organs and the carcass AuNP
24 contents increase between tenfold and hundred-fold it appears plausible that the passage across the
25 GIT-epithelium into blood occurs in a prolonged fashion compared to ABB translocation. 10% of the
26 circulating AuNP are rapidly removed by the liver but a tenth of those AuNP escape the liver and
27 become again redistributed in the organism.

33 The large differences in the biokinetics patterns of the identical AuNP after the three routes of
34 application clearly indicate that after each application the AuNP interact differently with the
35 constituents of the circulating blood and the vascular membranes of the secondary organs and tissues
36 although each AuNP size of this set of monodisperse of AuNP was dispersed in the same suspension.
37 Note however, two major differences between IV-injection versus IT-instillation or gavage are the
38 AuNP dose and dose rate in blood circulation although the applied AuNP doses were the same at all
39 three applications. But during IV-injection the AuNP suspension is injected as a bolus into the tail vein
40 within 20-30 sec while after IT-instillation and after gavage the crossing of the ABB or GIT-epithelium,
41 respectively, is prolonged over the first few hours and the amount of AuNP which crossed either
42 membrane is 2-3 orders of magnitude lower than after IV-injection. Even the contributions of pathways
43 across either membrane are unclear: after IT-instillation AuNP were found in endothelial cells of
44 alveolar vascular vesicles (Geiser 2010) but AuNP may well enter lymphatic drainage before entering
45 circulation which will likely take more time than just crossing through vascular endothelial cells. There
46 are doubts within the scientific GIT-physiology community that there is a direct entry across the GIT
47 epithelium into blood vessels (Powell 2010) and lymphatic pathways prior to the entry into circulation
48
49
50
51
52
53
54
55
56
57
58
59
60
61
62
63
64
65

1 are considered to be more realistic. The latter would be congruent with the delayed AuNP arrival in
2 blood causing a steep increase in blood and most organs and tissues between 1h and 24h (Fig. 24).

3 The role of rapidly binding serum biomolecules and/or proteins to the AuNP surface, particularly, that
4 of opsonin molecules are intensely discussed in the community but no quantitative data on the
5 trapping contribution of individual molecules are yet determined based on in vivo studies (Monopoli
6 2013, Zarschler 2016, Docter 2015). Furthermore, what is the role of cellular blood constituents like
7 monocytes, leucocytes, thrombocytes, erythrocytes, etc. interacting with the floating AuNP? Why do
8 cells of the mononuclear phagocytic system (MPS) interact at so different rates of interactions in
9 different organs, like liver versus spleen, kidneys, etc.? The lack of knowledge hampers strongly
10 nanomedicinal drug applications in diagnostics and therapy.
11
12
13
14
15
16
17
18
19
20

21 **Fig 24** Biokinetics patterns of Au18MS between one and 24 hours after IT-instillation, gavage or IV-
22 injection in liver, spleen, kidneys (upper panels) and in brain, remaining carcass and blood (lower
23 panels). IV-injection fractions are relative to ID; fractions of IT-instillation or gavage are normalized to
24 the AuNP fraction which had crossed the ABB or GIT-epithelium, respectively, into circulation for
25 subsequent accumulation. Note, in all organs and the carcass the AuNP content in the residual blood
26 volume of each organ was estimated and subtracted; therefore, the data present AuNP retained in the
27 tissues of each organ. Mean \pm SEM, n = 4 rats for each time point.
28
29
30
31
32
33
34

35 The physicochemical NP properties play a pivotal role in the biokinetics fate: In Figure 25 the AuNP size
36 dependent total translocation into blood is shown by integration over all accumulated AuNP in
37 secondary organs and tissues after IT-instillation and gavage. After both applications there is a linear
38 size-dependent decline from the smallest 1.4 nm particle (Au1.4MS) to 80 nm particle (Au80MS). After
39 IT-instillation translocation declines over almost two orders of magnitude and the decline is
40 proportional to the inverse of the AuNP diameter as indicated by the close to unity slope of the
41 regression line in Figure 25. This parameter represents the specific AuNP surface area (surface area
42 (μm^2) per volume (μm^3)); in other words, the translocation across the air-blood-barrier (ABB) declines
43 with declining specific surface area (SSA). However, this SSA pattern does no longer apply for the 200
44 nm AuNP after IT-instillation since it is significantly above the regression line. Whether this distinction
45 supports the current upper size limit of 100nm of nanoparticles versus larger sized particles may be an
46 interesting hint but needs certainly more specific analyses. After gavage, AuNP absorption declines 50-
47 fold with increasing AuNP diameter; but in contrast to IT-instillation the slope of the regression line of
48 absorption across the gut epithelium is no longer unity (i.e. SSA proportional) but about half of it (SSA
49 $\propto d^{-0.65}$). Here the 200 nm AuNP are fitting to the regression of the AuNP size decline. A physiological
50
51
52
53
54
55
56
57
58
59
60
61
62
63
64
65

1 explanation of these observations is lacking but it appears plausible that interactions of AuNP with
2 molecular and cellular constituents of blood as well as with MPS cells of the various organs and tissues
3 is surface-area dependent, i.e. the larger the surface area per NP volume or mass is the more molecular
4 binding reactions between the AuNP surface and the receptor molecules of cell membranes can take
5 place. Since AuNP in the circulation are likely not “naked” but coated by serum molecules within
6 seconds to minutes these binding reactions are modulated by the coating molecules rather than the
7 simple gold surface of AuNP. This increases the possible options of reactions tremendously – which
8 complicates disentangling the role of individual molecule types – but the rate and the capacity by the
9 large number of reactions accelerate largely leading to an effective defense line of the organism.
10
11
12
13
14
15
16
17
18

19 **Fig 25** Twenty-four-hour translocation across the ABB (upper left panel) or absorption across the gut
20 epithelium (upper right panel) respectively, given as percentage of initially applied dose (ID) of a suite
21 on monodisperse AuNP ranging from 1.4nm to 200nm after either IT-instillation or after gavage
22 (Kreyling 2014, Hirn 2011). A regression line and corresponding equation estimated for 1.4 nm to 80
23 nm AuNP are added. The lower panels confirm that this inverse size dependency results from liver,
24 spleen and carcass as indicated by their parallel gradient to the trend line taken from their respective
25 upper panels. Mean \pm SEM data of n=4 rats for each AuNP size. Note that the AuNP tested are TPPMS
26 stabilized except the 2.8nm AuNP, which are stabilized with thioglycolic acid (TGA) exhibiting a
27 terminal carboxyl group (COO⁻).
28
29
30
31
32
33
34
35
36

37 The lower panels of Figure 25 show that the size dependent total accumulation is maintained by liver,
38 spleen and the remaining carcass (comprising of the skeleton and soft tissues (like muscle, skin, fat
39 etc.) since after IT-instillation and gavage the size-dependent translocation / absorption runs parallel
40 to the trend lines taken from Figure 25. Both size dependencies are very different from that after IV-
41 injection (panel C). In this plot showing a linear y-axis it becomes clear that the smaller the AuNP
42 become the lower their retention in liver which is quite the opposite of SSA proportionality suggesting
43 either the limits of the trapping capacity of Kupffer cells for the huge number of 1.4 or 2.8 nm AuNP
44 or a different physiological trapping mechanism.
45
46
47
48
49
50
51
52

53 When normalizing translocation / absorption in liver, spleen and carcass not as a fraction of ID of IT-
54 instillation or gavage but of the amount of AuNP which had actually entered the circulation followed
55 by accumulation then the AuNP size dependency between 1.4 nm and 80 nm disappears grossly in liver
56 and spleen (Figure 26); this indicates that the larger the AuNP are the less they translocate / absorb
57 across the ABB / GIT epithelium, respectively, as already shown in Figure 22. The AuNP size
58
59
60
61
62
63
64
65

1
2
3
4
5
6
7
8
9
10
11
12
13
14
15
16
17
18
19
20
21
22
23
24
25
26
27
28
29
30
independency holds also for the AuNP accumulation after IV-injection on a logarithmic y-axis. Note however, that both, liver and spleen fractions after IT-instillation or gavage are tenfold lower than after IV-injection. More than 50% of the AuNP which had crossed either ABB or the GIT-epithelium accumulate in the remaining carcass also grossly AuNP size independent; while after IV-injection the AuNP size-dependent accumulation in the carcass decreases almost 100-fold from 1.4 nm to 80 nm suggesting that the latter application triggers different mechanisms of accumulation and/or retention when compared to IT-instillation or gavage.

31
32
33
34
35
36
37
38
39
40
41
42
43
44
45
46
47
48
49
50
51
52
53
54
55
56
57
58
59
60
61
62
63
64
65
Fig 26 Size-dependent 24-hour retentions in liver, spleen and carcass as percentage of those AuNP which had entered the circulation after crossing the ABB or GIT-epithelium (panels A + B) in order to directly compare with the retentions after IV-injection given as percent of ID (panel C) (Kreyling 2014, Schleh 2012, Hirn 2011). Data of 200 nm AuNP are not shown. Note that the AuNP tested are TPPMS stabilized except the 2.8nm AuNP, which are stabilized with thioglycolic acid (TGA) exhibiting a terminal carboxyl group (COO⁻).

7.3 Biokinetics fate depends on pre-engineered AuNP-protein-conjugates (albumin versus Apo-E)

31
32
33
34
35
36
37
38
39
40
41
42
43
44
45
46
47
48
49
50
51
52
53
54
55
56
57
58
59
60
61
62
63
64
65
In order to challenge the role of selected proteins tightly bound on the AuNP surface we crafted conjugates of either 15 nm or 80 nm monodisperse, ¹⁹⁸Au-radiolabeled AuNP with either albumin or apo-lipoprotein E (ApoE) prior to intravenous injection into the tail-vein of adult healthy female C57Bl/6 mice and followed the biokinetics from 30 min to 19 hours and 48 hours (Schäffler 2014). Citrate-coated AuNP served as particle controls. For tight protein binding a double layer methodology was applied using two polyelectrolyte molecules (polystyrene sulfonate (PSS) and poly-allylamine hydrochloride (PAH)) in between the AuNP surface and the protein (Sousa 2010).

In Figure 27 accumulation of 15 nm core diameter AuNP in liver, spleen, lungs, brain and remaining carcass are shown during 48 hours. The citrate-coated AuNP showed the same biokinetics patterns in mice as those of the sulfonated triphenyl-phosphine-coated 18 nm AuNP in rats (Figures 22+23); i.e. liver retention dominated by far retention in all other organs and the carcass. However, for both HSA-conjugated AuNP (Alb-AuNP) and ApoE-conjugated AuNP (ApoE-AuNP) only about 50% or 70%, respectively, were retained in the liver. About 20% of both conjugates were retained in the spleen and another 20% of Alb-AuNP were found in the lungs; i.e. retentions increased at least tenfold compared to the control-AuNP. In the remaining carcass (comprising of skeleton, muscles, connective tissue, fat, skin, etc.) Alb-AuNP retention was 10% and that of ApoE-AuNP was 5% which accounted for a tenfold or fivefold increase compared to the control-AuNP. Although AuNP-conjugate retentions in the brain

1 were below 0.1% they were 100-fold higher (Alb-AuNP) or tenfold (ApoE-AuNP), respectively, than that
2 of the 15 nm control-AuNP. The 80 nm AuNP-conjugates showed less pronounced but trend-wise
3 similar differences compared the 80 nm control-AuNP. In summary these results strongly suggest a
4 pivotal role of tightly bound HSA or ApoE on the biokinetics fate of AuNP. However, we cannot exclude
5 that either of the double layer fixed proteins stayed on the AuNP surface or may have been exchanged
6 to unknown extends by serum proteins. Therefore, even this rigid study design does not provide a
7 clear-cut answer which fraction of purely coated Alb-AuNP or ApoE-AuNP are retained in which organ
8 or tissue.
9
10
11
12
13
14
15
16
17

18 **Fig 27** Retention kinetics and of alb-AuNP, apoE-AuNP, and cit-AuNP (15 nm core diameter) in murine
19 liver, spleen, lungs, brain and carcass are determined at 30 min, 19 h and 48 h after IV-injection
20 (Schäffler 2014). Mean \pm SD of AuNP fractions per injected dose; n = 4 for each time point.
21
22
23
24
25
26

27 **7.4 In vivo stability of crafted surface modifications on AuNP demonstrated by biokinetics analyses**

28 To show that even firmly grafted polymer shells around AuNP may degrade when injected into rats,
29 synthesized monodisperse, radioactively labeled gold nanoparticles (^{198}Au) and engineered with an
30 ^{111}In -labelled polymer shell around them were IV-injected (Kreyling 2015). Equal biokinetics of both
31 radiolabels would indicate in vivo stability of the nanoparticles, whereas different biodistributions
32 would indicate partial degradation. A shell of the amphiphilic polymer poly(isobutylene-alt-maleic
33 anhydride)-graft-dodecyl was wrapped around the Au core. The chelator 1,4,7,10-
34 tetraazacyclododecane-1,4,7,10-tetraacetic acid (DOTA) was integrated into the polymer shell and was
35 loaded with In (enriched with the radioactive isotope ^{111}In , which acted as the shell label). By
36 calculating the ^{111}In to ^{198}Au ratio for each organ and tissue and each time point, major differences
37 between the retentions of the two radioisotopes became evident (Figure 28). This differential behavior
38 particularly in blood and excretion indicated dissociation and removal of the ^{111}In label from the shell
39 of the initial AuNP which is more pronounced after 24 hours than after one hour. Further in vitro
40 studies suggest that degradation of the polymer shell is caused by proteolytic enzymes in the liver
41 (Kreyling 2015). These results show that even nanoparticles with high colloidal stability can change
42 their physicochemical properties in vivo.
43
44
45
46
47
48
49
50
51
52
53
54
55
56
57
58
59
60
61
62
63
64
65

Fig 28 Ratios of ^{111}In shell to $^{198}\text{AuNP}$ radiolabel in each organ and tissue 1 h and 24 h after IV-injection (Kreyling 2015). AuNP (core diameter 5 nm) with a ^{198}Au core radiolabel grafted with a polymeric, ^{111}In radiolabeled shell were intravenously injected into the tail vein of Wistar–Kyoto rats and their radioactivities were determined in different organs and tissues. The ratios of retentions, given as mean data (\pm SEM), are denoted as percent of the total radioactivity for the respective radioisotope ($n = 4$ animals per data point). ‘Remainder’ represents radiolabels found in the rest of the carcass after sampling of organs (e.g. muscles, connective tissue, fat, skin and skeleton). ‘GIT + feces’ represents the radiolabels found in the gastrointestinal tract and in feces (note that after 1 h no radiolabels were found in feces). ‘Blood’ represents the total content of radiolabels, as calculated from the measured content in the blood sample and the estimate of the total blood volume. The data show that more ^{111}In shell labels than ^{198}Au core labels were detected in blood, urine, and GIT and feces at any time point. Reprinted by permission from Macmillan Publishers Ltd: Nature Nanotechnology Kreyling 2015 copyright (2015).

7.5 Size dependent AuNP crossing of the placenta into fetuses of pregnant rats

Since we have shown above that AuNP can cross various cellular and organ membranes the question arose whether AuNP can cross the placental membrane entering fetuses during pregnancy. Therefore we IV-injected a subset (1.4 nm, 18 nm, 80 nm) of the suite of different sized AuNP discussed above into the tail vein of pregnant rats in their third trimester (Semmler-Behnke 2014). The biodistribution after 24 hours only marginally differed from the non-pregnant control rats; therefore they correspond grossly to the data given in the Figures 22-26 above. Figure 27 shows that the applied AuNP accumulate in the uterine wall, the placenta, umbilical cords and the amniotic fluid after IV-injection; and eventually they can reach fetuses in a size dependent manner. However, even with our highly sensitive radio-analytical methodology we were not able to find 80 nm AuNP in the fetuses. A schematic sketch illustrates our observations showing that all three sizes of AuNP can cross the amniotic membrane which is surrounded by the uterine fluid being in exchange with maternal blood; this amniotic membrane crossing occurs by diffusion and/or active cellular transport mechanisms. But only 1.4 nm and 18 nm AuNP can also cross the placental barrier entering fetal blood circulation and hence the organism of the fetus. Interestingly the trophoblastic canalicular structure of the placenta prohibits the penetration of 80 nm AuNP into the fetal blood circulation. Furthermore, only the very small 1.4 nm AuNP in the amniotic fluid can cross the fetal skin but not the larger AuNP.

1
2
3
4
5
6
7
8
9
10
11
12
13
14
15
16
17
18
19
20
21
22
23
24
25
26
27
28
29
30
31
32
33
34
35
36
37
38
39
40
41
42
43
44
45
46
47
48
49
50
51
52
53
54
55
56
57
58
59
60
61
62
63
64
65

Fig 29 Retained fractions of IV-injected 1.4 nm, 18 nm or 80 nm monodisperse AuNP found after 24 hours in blood, uterus, placenta and fetuses of pregnant rats (Semmler-Behnke 2014). Data are mean fractions \pm SEM, n = 4 rats per AuNP size. At the left side a sketch illustrating AuNP pathways from the maternal blood towards the fetus. Figure reprinted from Semmler-Behnke 2014.

7.6 Disagglomeration dependent biokinetics of inhaled 40 nm AuNP consisting either of 7 nm or 20 nm primary AuNP

In many nanomedicinal or nanotechnological AuNP applications not primary AuNP but agglomerates of primary AuNP are likely to be used. When those agglomerates will enter the body the question arises whether these agglomerates stay intact or disagglomerate in the organism. (Note any disaggregation of more firmly bound aggregates by chemical bonds is less likely.) This is important since smaller AuNP distribute differently than larger AuNP as shown above in Figures 22+25+29. This was demonstrated in comparative inhalation exposures of rats which either inhaled Au-agglomerates of 7 nm primary AuNP or 20 nm primary AuNP (Balasubramanian 2013). Suspensions of either primary AuNP were nebulized yielding airborne Au-agglomerates of about the same size, 46 nm and 42 nm, respectively, such that the deposition of the inhaled Au-agglomerates was identical in the lungs. As a result the Au-agglomerates comprising of 7 nm primary AuNP (Au-Agg(7 nm)) contained 23-fold more AuNP than those (Au-Agg(20 nm)) comprised of the 20 nm AuNP. Inhalation exposures were performed during 15 days (for 6 h/d, 5 d/wk for 3 wks) and the rats were analyzed 2 days after last exposure day by ICP-MS analyses of the dissected organs and tissues. After both exposures about 90% Au-mass remained in the lungs and 7.6% versus 8.4%, respectively, were observed in the gastro-intestinal-tract (GIT) and feces as a result of fast mucociliary clearance from the conducting airways; while 2% of the (Au-Agg(7 nm)) versus 0.3% of the (Au-Agg(20 nm)) were translocated across the ABB into blood and accumulated subsequently in secondary organs and tissues. Figure 30 shows that all secondary organs and a muscle sample contain about four-times up to eight-times more Au-mass after the inhalation of (Au-Agg(7 nm)) when compared to that of (Au-Agg(20 nm)). In contrast the ratio of Au-mass in the lungs is about unity. These data demonstrate clearly that the (Au-Agg(7 nm)) disagglomerate to a greater extent and the disagglomerated primary 7 nm AuNP or small clusters of those cross the air-blood barrier of the lungs more readily leading to higher accumulations than primary 20 nm AuNP in all organs and tissues studied. Muscular tissue like heart and the muscle sample accumulate as much as the brain being double that of the other secondary organs studied.

1
2
3
4
5
6
7
8
9
10
11
12
13
14
15
16
17
18
19
20
21
22
23
24
25
26
27
28
29
30
31
32
33
34
35
36
37
38
39
40
41
42
43
44
45
46
47
48
49
50
51
52
53
54
55
56
57
58
59
60
61
62
63
64
65

Fig 30 Ratios of retained Au-masses in lungs, secondary organs and a muscle sample after inhalation exposure to Au-Agg(7 nm) versus Au-Agg(20 nm). Au-masses were determined by Inductive-Coupled-Plasma-Mass-Spectroscopy (ICP-MS). Data are ratios of mean Au-masses of n=7 rats per exposure (Balasubramanian 2013).

8. Summary

This review has illustrated that ultrasmall AuNP can exhibit cytotoxic profile, when the stabilizing ligands allows for direct access to the gold surface either for the direct interaction with biomolecules or for catalytic activity of the unshielded gold surface. Furthermore, it was shown that ultrasmall AuNP exhibit significantly different biodistribution, and enhanced circulation times compared to larger AuNP. In contrast to larger particles, which relatively fast accumulated in the liver, ultrasmall AuNPs distribute over all other organs as well. The summary of these finding may stimulate the discussion among different disciplines related to (nano)toxicology about possible therapeutic applications of ultrasmall AuNPs that may be anticipated in the future.

References

- 1 Alkilany AM, Murphy CJ (2010) Toxicity and cellular uptake of gold nanoparticles: what we have
2 learned so far? *J Nanopart Res* 12:2313-2333. doi:10.1007/s11051-010-9911-8
3
4
5 Amsterdam A, Nissen RM, Sun Z, Swindell EC, Farrington S, Hopkins N (2004) Identification of 315 genes
6 essential for early zebrafish development. *Proc Natl Acad Sci* 101(35):12792-12797. doi:
7 10.1073/pnas.0403929101
8
9
10 Balasubramanian SK, Poh KW, Ong CN, Kreyling WG, Ong WY, Yu LE (2013) The effect of primary
11 particle size on biodistribution of inhaled gold nano-agglomerates. *Biomaterials* 34:5439-52.
12 doi:10.1016/j.biomaterials.2013.03.080
13
14
15 Bezryadin A, Dekker C, Schmid G (1997) Electrostatic trapping of single conducting nanoparticles
16 between nanoelectrodes. *Appl Phys Lett* 71(9):1273-1275. doi: 10.1063/1.119871
17
18
19 Boda SK, Broda J, Schiefer F, Weber-Heynemann J, Hoss M, Simon U, Basu B, Jahnen-Dechent W (2015)
20 Cytotoxicity of Ultrasmall Gold Nanoparticles on Planktonic and Biofilm Encapsulated Gram-Positive
21 Staphylococci. *Small* 11:3183-3193. doi:10.1002/sml.201403014
22
23
24 Bogart LK, Pourroy G, Murphy CJ, Puntès V, Pellegrino T, Rosenblum D, Peer D, Lévy R (2014)
25 Nanoparticles for Imaging, Sensing, and Therapeutic Intervention. *ACS Nano* 8(4):3107-3122.
26 doi:10.1021/nn500962q
27
28
29 Boyen HG, Kästle G, Weigl F, Koslowski B, Dietrich C, Ziemann P, Spatz JP, Riethmüller S, Hartmann C,
30 Möller M, Schmid G, Garnier MG, Oelhafen P (2002) Oxidation-resistant gold-55 clusters. *Science*
31 297(5586):1533-1536. doi:10.1126/science.1076248
32
33
34 Broda J, Schmid G, Simon U (2014) Size- and Ligand-Specific Bioresponse of Gold Clusters and
35 Nanoparticles : Challenges and Perspectives. In: Mingos DMP (ed) *Gold Clusters, Colloids and*
36 *Nanoparticles I*, Springer International Publishing Switzerland, pp 189-241.
37
38
39 Broda J, Küster A, Westhues S, Fahrenkamp D, Vogg A T J, Steitz J, Mottaghy F M, Müller-Newen G,
40 Simon U (2016a) Assessing the Intracellular Integrity of Phosphine-Stabilized Ultrasmall Cytotoxic
41 Gold Nanoparticles Enabled by Fluorescence Labeling. *Adv Healthcare Mater* 5:3118-3128.
42 doi:10.1002/adhm.201600892
43
44
45 Broda J, Setzler J, Leifert A, Steitz J, Benz R, Simon U, Wenzel W (2016b) Ligand-lipid and ligand-core
46 affinity control the interaction of gold nanoparticles with artificial lipid bilayers and cell membranes.
47 *Nanomedicine* 12(5):1409-19. doi:10.1016/j.nano.2015.12.384
48
49
50 Chi L, Hartig M, Drechsler T, Schwaack T, Seidel C, Fuchs H, Schmid G (1998) Single-electron tunneling
51 in Au55 cluster monolayers. *Appl Phys A* 66(Suppl 1): S187-S190. doi:10.1007/s003390051127
52
53
54 Chowdhury MH, Aslan K, Malyn SN, Iakowicz JR, Geddes CD (2006) Metal-enhanced
55 chemiluminescence: Radiating plasmons generated from chemically induced electronic excited
56 states. *Appl Phys Lett* 88:173104. doi:10.1063/1.2195776
57
58
59
60
61
62
63
64
65

- 1
2
3
4
5
6
7
8
9
10
11
12
13
14
15
16
17
18
19
20
21
22
23
24
25
26
27
28
29
30
31
32
33
34
35
36
37
38
39
40
41
42
43
44
45
46
47
48
49
50
51
52
53
54
55
56
57
58
59
60
61
62
63
64
65
- Cluskey PD, Newport RJ, Benfield RE, Gurman SJ, Schmid G (1993) An EXAFS study of some gold and palladium cluster compounds. *Z Phys D - Atoms, Molecules and Clusters* 26(Suppl 1):8. doi:10.1007/BF01425601
- Corain B, Schmid G, Toshima N (2008) *Metal Nanoclusters in Catalysis and Materials Science: The Issue of Size Control*. Elsevier Science.
- Crooks RM, Zhao M, Sun L, Chechik V, Yeung LK (2001) Dendrimer-Encapsulated Metal Nanoparticles: Synthesis, Characterization, and Applications to Catalysis. *Acc Chem Res* 34(3):181-190. doi:10.1021/ar000110a
- Daniel MC, Astruc D (2004) Gold Nanoparticles: Assembly, Supramolecular Chemistry, Quantum-Size-Related Properties, and Applications toward Biology, Catalysis, and Nanotechnology. *Chem Rev* 104:293-346. doi:10.1021/cr030698+
- Demann ET, Stein PS, Haubenreich JE (2005) Gold as an implant in medicine and dentistry. *J Long Term Eff Med Implants* 15(6):687-698. doi:10.1615/JLongTermEffMedImplants.v15.i6.100
- Docter, D, Westmeier, D, Markiewicz, M, Stolte, S, Knauer, SK & Stauber, RH (2015). The nanoparticle biomolecule corona: lessons learned - challenge accepted? *Chem Soc Rev* 44:6094-6121. DOI: 10.1039/c5cs00217f
- Dreaden EC, Alkilany AM, Huang X, Murphy CJ, El-Sayed MA (2012) The golden age: gold nanoparticles for biomedicine. *Chem Soc Rev* 41:2740-2779. doi:10.1039/C1CS15237H
- EFSA Panel on Food Additives and Nutrient Sources added to Food (2016) Scientific Opinion on the re-evaluation of gold (E175) as a food additive. *EFSA Journal* 14(1):4362(43pp). doi:10.2903/j.efsa.2016.436
- El-Sayed MA (2003) Optical properties and ultrafast dynamics of metallic nanocrystals. *Annu Rev Phys Chem* 54:331-366. doi: 10.1146/annurev.physchem.54.011002.103759
- Esumi K, Tano T, Meguro K (1989) Preparation of organo palladium particles from thermal decomposition of its organic complex in organic solvents. *Langmuir* 5(1):268-270. doi:10.1021/la00085a051
- Esumi K, Tano T, Torigoe K, Meguro K (1990) Preparation and characterization of bimetallic palladium-copper colloids by thermal decomposition of their acetate compounds in organic solvents. *Chem Mater* 2:564-567. doi:10.1021/cm00011a019
- Esumi K, Zuzuki M, Tano T, Torigoe K, Meguro K (1991) Dispersion of uniformly sized palladium particles in organic solvents. *Colloids Surf* 55:9-14. doi:10.1016/0166-6622(91)80078-3
- Esumi K, Sadakane O, Torigoe K, Meguro K (1992) Preparation of platinum particles by thermal decomposition of platinum complex in organic solvent. *Colloids Surf* 62(3):255-257. doi:10.1016/0166-6622(92)80008-P
- Esumi K, Sato N, Torigoe K, Meguro K (1992) Size control of gold particles using surfactants. *J Colloid Interface Sci* 149(1):295-298. doi:10.1016/0021-9797(92)90417-K

- 1
2
3
4
5
6
7
8
9
10
11
12
13
14
15
16
17
18
19
20
21
22
23
24
25
26
27
28
29
30
31
32
33
34
35
36
37
38
39
40
41
42
43
44
45
46
47
48
49
50
51
52
53
54
55
56
57
58
59
60
61
62
63
64
65
- FDA (2005) ICH S7B Guideline of FDA (Food and Drug Administration, Rockville, MD).
<https://www.fda.gov/downloads/Drugs/GuidanceComplianceRegulatoryInformation/Guidances/ucm074963.pdf>
- Fu X, Wang, Y, Wu N, Gui L (2002) Shape-Selective Preparation and Properties of Oxalate-Stabilized Pt Colloid. *Langmuir* 18(12): 4619-4624. doi:10.1021/la020087x
- Geiser M, Kreyling WG (2010) Deposition and biokinetics of inhaled nanoparticles. Part Fibre Toxicol, 7:2(17pp). doi:10.1186/1743-8977-7-2
- Grzelczak M, Pérez-Juste J, Mulvaney P, Liz-Marzán LM (2008) Shape Control in Gold Nanoparticle Synthesis. *Chem Soc Rev* 37:1783-1791. doi:10.1039/b711490g
- Gutrath BS, Merckens C, Schiefer F, Englert U, Schmid G, Simon U (2013) Isolation, Optical Properties and Core Structure of a Water-soluble, Phosphine-stabilized [Au₉]³⁺ Cluster. *Z Naturforsch* 68b:569-574. doi:10.5560/ZNB.2013-3075
- Häkkinen H (2008) Atomic and electronic structure of gold clusters: understanding flakes, cages and superatoms from simple concepts. *Chem Soc Rev* 37:1847-1859. doi:10.1039/b717686b.
- Hammer B, Norskov JK(1995) Why gold is the noblest of all the metals? *Nature* 376 (6537): 238-240. doi:10.1038/376238a0
- He W, Kivork C, Machinani S, Morpew MK, Gail AM, Tesar DB, Tiangco NE, McIntosh JR, Bjorkman PJ (2007) A Freeze Substitution Fixation-Based Gold Enlarging Technique for EM Studies of Endocytosed Nanogold-Labeled Molecules. *J Struct Biol* 160(1):103-113. doi:10.1016/j.jsb.2007.07.004
- Henglein A (2000) Preparation and Optical Absorption Spectra of AuCorePtshell and PtcoreAushell Colloidal Nanoparticles in Aqueous Solution. *J Phys Chem B* 104:2201-2203. doi:10.1021/jp994300i
- Hirn S, Semmler-Behnke M, Schleh C, Wenk A, Lipka J, Schaffler M, Takenaka S, Moller W, Schmid G, Simon U, Kreyling WG (2011) Particle size-dependent and surface charge-dependent biodistribution of gold nanoparticles after intravenous administration. *Eur J Pharm Biopharm* 77:407-16. doi:10.1016/j.ejpb.2010.12.029
- Homberger M, Simon U (2010) On the application potential of gold nanoparticles in nanoelectronics and biomedicine. *Phil Trans R Soc A* 368:1405-1453. doi:10.1098/rsta.2009.0275
- Jia Y-P, Ma B-Y, Wie X-W, Zhi-Yong Qian Z-Y (2017) The in vitro and in vivo toxicity of gold nanoparticles. *Chin Chem Lett* doi:10.1016/j.ccllet.2017.01.021
- Ke X, Wang D, Chen C, Yang A, Han Y, Ren L, Li D, Wang H (2014) Co-enhancement of fluorescence and singlet oxygen generation by silica-coated gold nanorods core-shell nanoparticle. *Nanoscale Res Lett* 9:666. doi:10.1186/1556-276X-9-666
- Khlebtsov N, Dykman L (2011) Biodistribution and toxicity of engineered gold nanoparticles: a review of in vitro and in vivo studies. *Chem Soc Rev* 40:1647-1671. doi:10.1039/C0CS00018C

- 1 Kosmehl T, Otte JC, Yang L, Legradi J, Bluhm K, Zinsmeister C, Keiter SH, Reifferscheid G, Manze W,
2 Braunbeck T, Strähle U, Hollert H (2012) A combined DNA-microarray and mechanism-specific
3 toxicity approach with zebrafish embryos to investigate the pollution of river sediments. *Reprod*
4 *Toxicol* 33:245-253. doi:10.1016/j.reprotox.2012.01.005
5
6
7 Kreyling WG, Semmler-Behnke M, Takenaka S, Moller W (2013) Differences in the biokinetics of
8 inhaled nano- versus micrometer-sized particles. *Acc Chem Res* 46:714-22. doi:10.1021/ar300043r
9
10 Kreyling WG, Hirn S, Möller W, Schleh C, Wenk A, Celik G, Lipka J, Schäffler M, Haberl N, Johnston BD,
11 Sperling R, Schmid G, Simon U, Parak WJ, Semmler-Behnke M (2014) Air–Blood Barrier
12 Translocation of Tracheally Instilled Gold Nanoparticles Inversely Depends on Particle Size. *ACS*
13 *Nano* 8:222-223. doi:10.1021/nn403256v
14
15
16
17 Kreyling WG, Abdelmonem AM, Ali Z, Alves F, Geiser M, Haberl N, Hartmann R, Hirn S, de Aberasturi
18 DJ, Kantner K, Khadem-Saba G, Montenegro JM, Rejman J, Rojo T, de Larramendi IR, Ufartes R,
19 Wenk A, Parak WJ (2015) In vivo integrity of polymer-coated gold nanoparticles. *Nat Nanotechnol*
20 *10*:619-623. doi:10.1038/nnano.2015.111
21
22
23
24 Leifert A, Pan Y, Kinkeldey A, Schiefer F, Setzler J, Scheel O, Lichtenbeld H, Schmid G, Wenzel W,
25 Jahnen-Dechent W, Simon U (2013) Differential hERG ion channel activity of ultrasmall gold
26 nanoparticles. *Proc Natl Acad Sci* 110(20):8004-8009. doi: 0.1073/pnas.1220143110
27
28
29
30 Leifert A, Yu Pan-Bartne Y, Simon U, Jahnen-Dechent W (2013) Molecularly stabilised ultrasmall gold
31 nanoparticles: synthesis, characterization and bioactivity. *Nanoscale* 5:6224-6242.
32 doi:10.1039/C3NR00916E
33
34
35
36 Lewinski N, Colvin V, Drezek R (2008) Cytotoxicity of Nanoparticles. *Small* 4(1):26-49.
37 doi:10.1002/smll.200700595
38
39
40 Li Y, Petroski J, El-Sayed MA (2000) Activation Energy of the Reaction between Hexacyanoferrate(III)
41 and Thiosulfate Ions Catalyzed by Platinum Nanoparticles. *J Phys Chem B* 104:1095.
42 doi:10.1021/jp002569s
43
44
45 Li W, Chen X (2015) Gold nanoparticles for photoacoustic imaging. *Nanomedicine* 10(2):299-320.
46 doi:10.2217/nnm.14.169
47
48
49 Liu Y, Meyer-Zaika W, Franzka S, Schmid G, Tsoli M, Kuhn H (2003) Gold-cluster degradation by the
50 transition of B-DNA into A-DNA and the formation of nanowires. *Angew Chem Int Ed* 42:2853.
51 doi:10.1002/anie.200250235
52
53
54 Marquis BJ, Love SA, Braun KL, Haynes CL (2009) Analytical methods to assess nanoparticle toxicity.
55 *Analyst* 134:425-439. doi:10.1039/b818082b
56
57
58
59 Mie G (1908) Beiträge zur Optik trüber Medien, speziell kolloidaler Metallösungen. *Ann Phys* 330:377-
60 445. doi:10.1002/andp.19083300302
61
62
63
64
65 Miller, MR, Raftis, JB, Langrish, JP, McLean, SG, Samutrtai, P, Connell, SP, Wilson, S, Vesey, AT, Fokkens,

- 1 PHB, Boere, AJF, Krystek, P, Campbell, CJ, Hadoke, PWF, Donaldson, K, Cassee, FR, Newby, DE,
2 Duffin, R, Mills, NL (2017), Inhaled Nanoparticles Accumulate at Sites of Vascular Disease, ACS
3 Nano, Article ASAP, doi: 10.1021/acsnano.6b08551
4
- 5 Monopoli, MP, Pitek, AS, Lynch, I & Dawson, KA (2013) Formation and characterization of the
6 nanoparticle-protein corona. *Methods Mol Biol*, 1025, 137-55. doi: 10.1007/978-1-62703-462-3_11
7
- 8 Narayanan R, El-Sayed MA (2004) Effect of Nanocatalysis in Colloidal Solution on the Tetrahedral and
9 Cubic Nanoparticle SHAPE: Electron-Transfer Reaction Catalyzed by Platinum Nanoparticles. *J Phys
10 Chem B* 108(18):5726-5733. doi:10.1021/jp0493780
11
- 12 Ohde H, Wai CM, Kim H, Kim J, Ohde M (2002) Hydrogenation of Olefins in Supercritical CO₂ Catalyzed
13 by Palladium Nanoparticles in a Water-in-CO₂ Microemulsion. *J Am Chem Soc* 124(17):4540-4541.
14 doi:10.1021/ja012232j
15
- 16 Pan Y, Neuss S, Leifert A, Fischler M, Wen F, Simon U, Schmid G, Brandau W, Jahnen-Dechent W (2007)
17 Size-dependent cytotoxicity of gold nanoparticles. *Small* 3(11):1941-1949.
18 doi:10.1002/sml.200700378
19
- 20 Pan Y, Leifert A, Ruau D, Neuss S, Bornemann J, Schmid G, Brandau W, Simon U, Jahnen-Dechent W
21 (2009) Gold nanoparticles of diameter 1.4 nm trigger necrosis by oxidative stress and mitochondrial
22 damage. *Small* 5(18):2067-76. doi:10.1002/sml.200900466
23
- 24 Pan Y, Leifert A, Graf M, Schiefer F, Thoröe-Boveleth S, Broda J, Halloran MC, Hollert H, Laaf D, Simon
25 U, Jahnen-Dechent W (2013) High-Sensitivity Real-Time Analysis of Nanoparticle Toxicity in Green
26 Fluorescent Protein-Expressing Zebrafish. *Small* 9: 863-869. doi:10.1002/sml.201201173
27
- 28 Powell, JJ, Faria, N, Thomas-Mckay, E & Pele, LC 2010. Origin and fate of dietary nanoparticles and
29 microparticles in the gastrointestinal tract. *J Autoimmun*, 34, J226-33.
30 doi:10.1016/j.jaut.2009.11.006
31
- 32 Reimers JR, Ford MJ, Marcuccio SM, Ulstrup J, Hush NS (2017) Competition of van der Waals and
33 chemical forces on gold-sulfur surfaces and nanoparticles. *Nature Reviews Chemistry* 1:0017.
34 doi:10.1038/s41570-017-0017
35
- 36 Rivera-Gil P, De Aberasturi DJ, Wulf V, Pelaz B, Del Pino P, Zhao Y, De La Fuente JM, De Larramend IR,
37 Teófilo Rojo T, Xing-Jie Liang X-J, Parak WJ (2013) The Challenge To Relate the Physicochemical
38 Properties of Colloidal Nanoparticles to Their Cytotoxicity. *Acc Chem Res* 46(3):743749.
39 doi:10.1021/ar300039j
40
- 41 Rizzo LY, Golombek SK, Mertens ME, Pan Y, Laaf D, Broda J, Jayapaul J, Möckel D, Subr V, Hennink WE,
42 Storm G, Simon U, Jahnen-Dechent W, Kiessling F, Lammers T (2013) In Vivo Nanotoxicity Testing
43 using the Zebrafish Embryo Assay. *J Mater Chem B Mater Biol Med*. 10(1): 3918-3925.
44 doi:10.1039/C3TB20528B.
45
46
47
48
49
50
51
52
53
54
55
56
57
58
59
60
61
62
63
64
65

- 1
2
3
4
5
6
7
8
9
10
11
12
13
14
15
16
17
18
19
20
21
22
23
24
25
26
27
28
29
30
31
32
33
34
35
36
37
38
39
40
41
42
43
44
45
46
47
48
49
50
51
52
53
54
55
56
57
58
59
60
61
62
63
64
65
- Rosi NL, Giljohann DA, Thaxton CS, Lytton-Jean AK, Han MS, Mirkin CA (2006) Oligonucleotide-modified gold nanoparticles for intracellular gene regulation. *Science* 312(5776):1027-1030. doi:10.1126/science.1125559
- Schaeublin NM, Braydich-Stolle LK, Schrand AM, Miller JM, Hutchison J, Schlager JJ, Hussain SM (2011) Surface charge of gold nanoparticles mediates mechanism of toxicity. *Nanoscale* 3(2):410-420. doi:10.1039/c0nr00478b
- Schäffler M, Sousa F, Wenk A, Sitia L, Hirn S, Schleh C, Haberl N, Violatto M, Canovi M, Andreozzi P, Salmona M, Bigini P, Kreyling WG, Krol S (2014) Blood protein coating of gold nanoparticles as potential tool for organ targeting. *Biomaterials* 35(10):3455-66. doi:10.1016/j.biomaterials.2013.12.100.
- Schleh C, Semmler-Behnke M, Lipka J, Wenk A, Hirn S, Schaffler M, Schmid G, Simon, U, Kreyling WG (2012) Size and surface charge of gold nanoparticles determine absorption across intestinal barriers and accumulation in secondary target organs after oral administration. *Nanotoxicology* 6(1):36-46. doi:10.3109/17435390.2011.552811.
- Schmid G, Pfeil R, Boese R, Bandermann F, Meyer S, Calis Gijs H M, van der Velden JWA (1981) Au₅₅[P(C₆H₅)₃]₁₂Cl₆ - ein Goldcluster ungewöhnlicher Größe. *Chem Ber* 114:3634-3642. doi:10.1002/cber.19811141116
- Schmid G. (1994) *Clusters and Colloids*. Wiley-VCH, Weinheim
- Schmid G, Corain B (2003) *Nanoparticulated Gold: Syntheses, Structures, Electronics, and Reactivities*. *Eur J Inorg Chem* 2003:3081-3098. doi:10.1002/ejic.200300187
- Schmid G (2004) *Nanoparticles*. Wiley-VCH, Weinheim
- Schmid G, Simon U (2005) Gold nanoparticles: assembly and electrical properties in 1-3 dimensions. *Chem Commun* 6:697-710. doi: 10.1039/B411696H
- Schmid G (2008) The relevance of shape and size of Au₅₅ clusters. *Chem Soc Rev* 37:1909-1930. doi:10.1039/B713631P
- Scholz S, Fischer S, Gündel U, Küster E, Luckenbach T, Voelker D (2008) The zebrafish embryo model in environmental risk assessment - applications beyond acute toxicity testing. *Environ Sci Pollut Res Int* 15(5):394-404. doi:10.1007/s11356-008-0018-z
- Semmler-Behnke M, Kreyling WG, Lipka J, Fertsch S, Wenk A, Takenaka S, Schmid G, Brandau W (2008) Biodistribution of 1.4- and 18-nm gold particles in rats. *Small* 4:2108-11. doi:10.1002/smll.200800922
- Semmler-Behnke M, Lipka J, Wenk A, Hirn S, Schaffler M, Tian F, Schmid G, Oberdorster G, Kreyling W (2014) Size dependent translocation and fetal accumulation of gold nanoparticles from maternal blood in the rat. *Part Fibre Toxicol* 11:33. doi:10.1186/s12989-014-0033-9
- Shaw III CF (1999) Gold-based therapeutic agents. *Chem Rev* 99(9):2589-2600. doi:10.1021/cr980431o

- 1
2
3
4
5
6
7
8
9
10
11
12
13
14
15
16
17
18
19
20
21
22
23
24
25
26
27
28
29
30
31
32
33
34
35
36
37
38
39
40
41
42
43
44
45
46
47
48
49
50
51
52
53
54
55
56
57
58
59
60
61
62
63
64
65
- Smith BA, Zhang JZ, Giebel U, Schmid G (1997) Direct probe of size-dependent electronic relaxation in single-sized Au and nearly monodisperse Pt colloidal nano-particles. *Chem Phys Lett* 270(1-2):139. doi:10.1016/S0009-2614(97)00339-4
- Soenen SJ, Manshian B, Montenegro JM, Amin F, Meermann B, Thiron T, Cornelissen M, Vanhaecke F, Doak S, Parak WJ, De Smedt S, Braeckmans K (2012) Cytotoxic Effects of Gold Nanoparticles: A Multiparametric Study. *ACS Nano* 6(7):5767-5783. doi:10.1021/nn301714n
- Sousa F, Mandal S, Garrovo C, Astolfo A, Bonifacio A, Latawiec D, Menk RH, Arfelli F, Huewel S, Legname G, Galla HJ, Krol S (2010) Functionalized gold nanoparticles: a detailed in vivo multimodal microscopic brain distribution study. *Nanoscale* 2(12):2826-34. doi:10.1039/c0nr00345j
- Sousa AA, Morgan JT, Brown PH, Adams A, Jayasekara MPS, Zhang G, Ackerson CJ, Kruhlak MJ, Leapman RD (2012) Synthesis, Characterization, and Direct Intracellular Imaging of Ultrasmall and Uniform Glutathione-Coated Gold Nanoparticles. *Small* 8: 2277-2286. doi:10.1002/smll.201200071
- Stone V, Miller MR, Clift MJ, Elder A, Mills NL, Møller P, Schins RP, Vogel U, Kreyling WG, Jensen KA, Kuhlbusch TA, Schwarze PE, Hoet P, Pietroiusti A, De Vizcaya-Ruiz A, Baeza-Squiban A, Tran CL, Cassee FR (2016) Nanomaterials vs Ambient Ultrafine Particles: an Opportunity to Exchange Toxicology Knowledge. *Environ Health Perspect*. doi:10.1289/EHP424
- Tano T, Esumi K, Meguro K (1989) Preparation of organopalladium sols by thermal decomposition of palladium acetate. *J Colloid Interface Sci* 133:530-533. doi:10.1016/S0021-9797(89)80069-4
- Tsoli M, Kuhn H, Brandau W, Esche H, Schmid G (2005) Cellular uptake and toxicity of Au₅₅ clusters. *Small* 841-844. doi:10.1002/smll.200500104
- Turner M, Golovko VB, Vaughan OP, Abdulkin P, Berenguer-Murcia A, Tikhov MS, Johnson BF, Lambert RM (2008) Selective oxidation with dioxygen by gold nanoparticle catalysts derived from 55-atom clusters. *Nature* 454:981-983. doi:10.1038/nature07194
- Tyo EC, Vajda S (2015) Catalysis by clusters with precise numbers of atoms. *Nat Nanotechnol* 10:577-588. doi:10.1038/nnano.2015.140
- Verma A, Stellacci F (2010) Effect of Surface Properties on Nanoparticle–Cell Interactions. *Small* 6:12-21. doi: 10.1002/smll.200901158.
- Yavuz MS, Cheng Y, Chen J, Cogley CM, Zhang Q, Rycenga M, Xie J, Kim C, Song KH, Schwartz AG, Wang LV, Xia Y (2009) Gold nanocages covered by smart polymers for controlled release with near-infrared light. *Nat Mater* 8:935-939. doi:10.1038/nmat2564
- Zarschler, K, Rocks, L, Licciardello, N, Boselli, L, Polo, E, Garcia, KP, De Cola, L, Stephan, H & Dawson, KA 2016. Ultrasmall inorganic nanoparticles: State-of-the-art and perspectives for biomedical applications. *Nanomedicine*, 12, 1663-701. doi: 10.1016/j.nano.2016.02.019
- Zhang H, Schmid G, Hartmann U (2003) Reduced Metallic Properties of Ligand-Stabilized Small Metal Clusters. *Nano Lett* 3(3):305-307. doi:10.1021/nl0258980

Cell Line		IC ₅₀ cisplatin, 72 h [μM]	IC ₅₀ Au ₅₅ , 24 h [μM]
MC3T3-E1	Bone cells	26.10±1.27	1.65±0.14
U-2OS	Osteosarcoma	11.17±2.02	0.64±0.04
SK-ES-1	Osteosarcoma	0.79±0.17	1.03±0.18
MOR/P	Lung cancer cells	3.30±0.30	2.10±0.10
MOR/CPR	Lung cancer cells	7.10±1.2	2.50±0.10
CCD-919Sk	Fibroblast cells	0.45±0.10	0.62±0.07
BLM	Metastatic melanoma	54.70±7.60	0.30±0.10
M V3	Metastatic melanoma	>50	0.24±0.02
SMel-28	Melanoma	15.60±2.26	1.12±0.16
HeLa	Cervical cancer cells	7.93±0.95	2.29±0.10
Hek-12	Kidney cancer cells ^[*]	20.13±6.0	0.63±0.02

[*] Kidney cancer cells transformed with adenovirus.

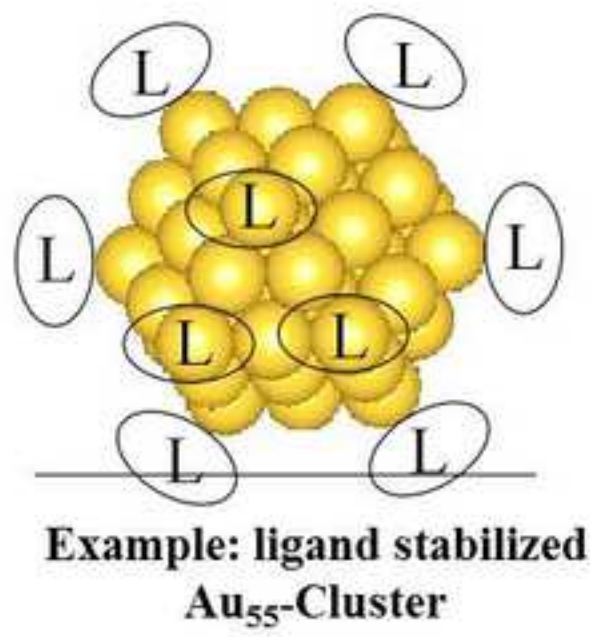
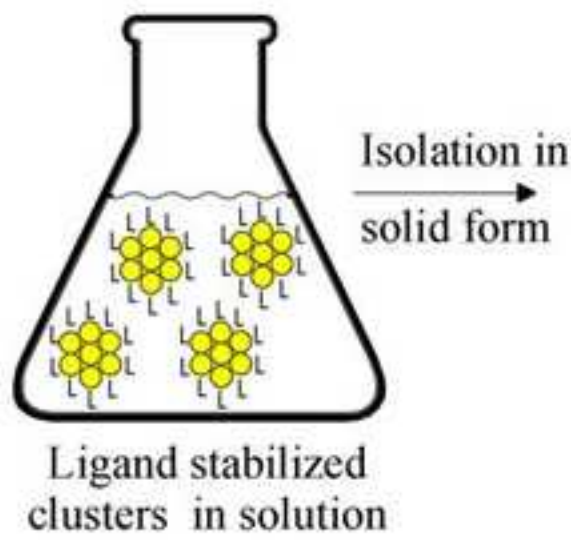
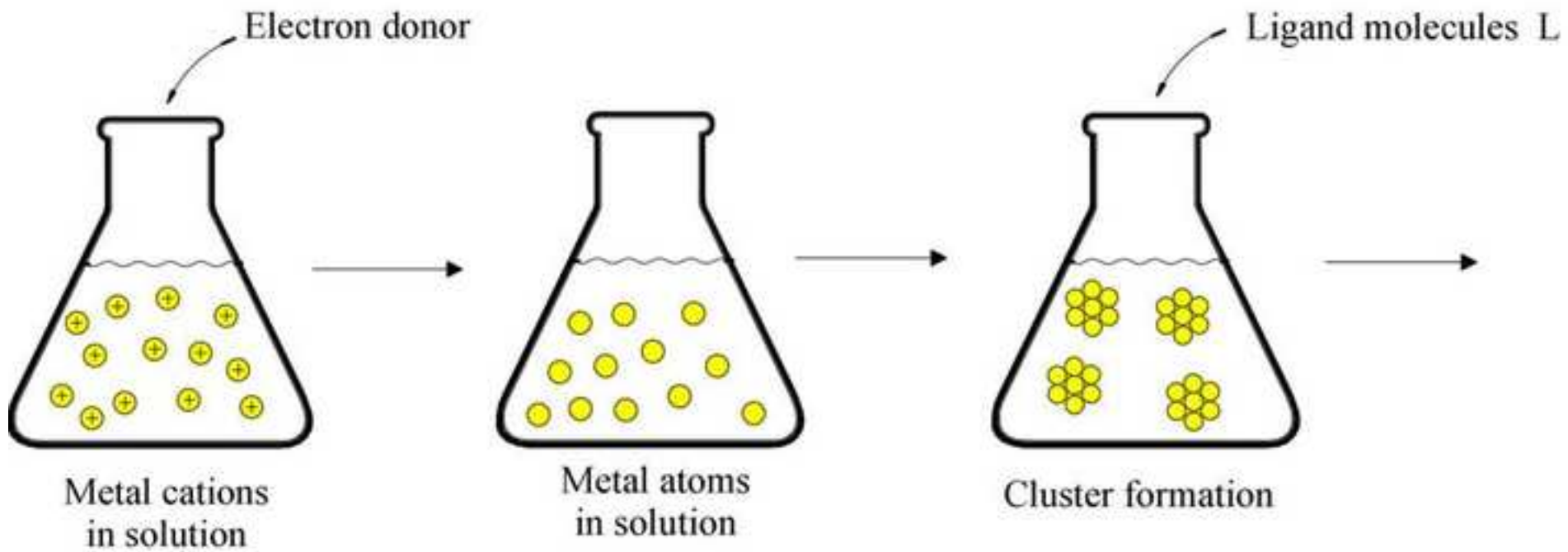
Sample	Applied Au Concentration	Internalized AuNPs per cell	Cellular Uptake Efficiency / %
Au1.4MS	1 μ M	$1.9 * 10^5$	2.5
Au1.4MS	75 μ M	$9.5 * 10^6$	1.7
Au1.4MS/CBE	1 μ M	$1.9 * 10^5$	2.7
Au1.4MS/CBE	75 μ M	$1.5 * 10^7$	2.7

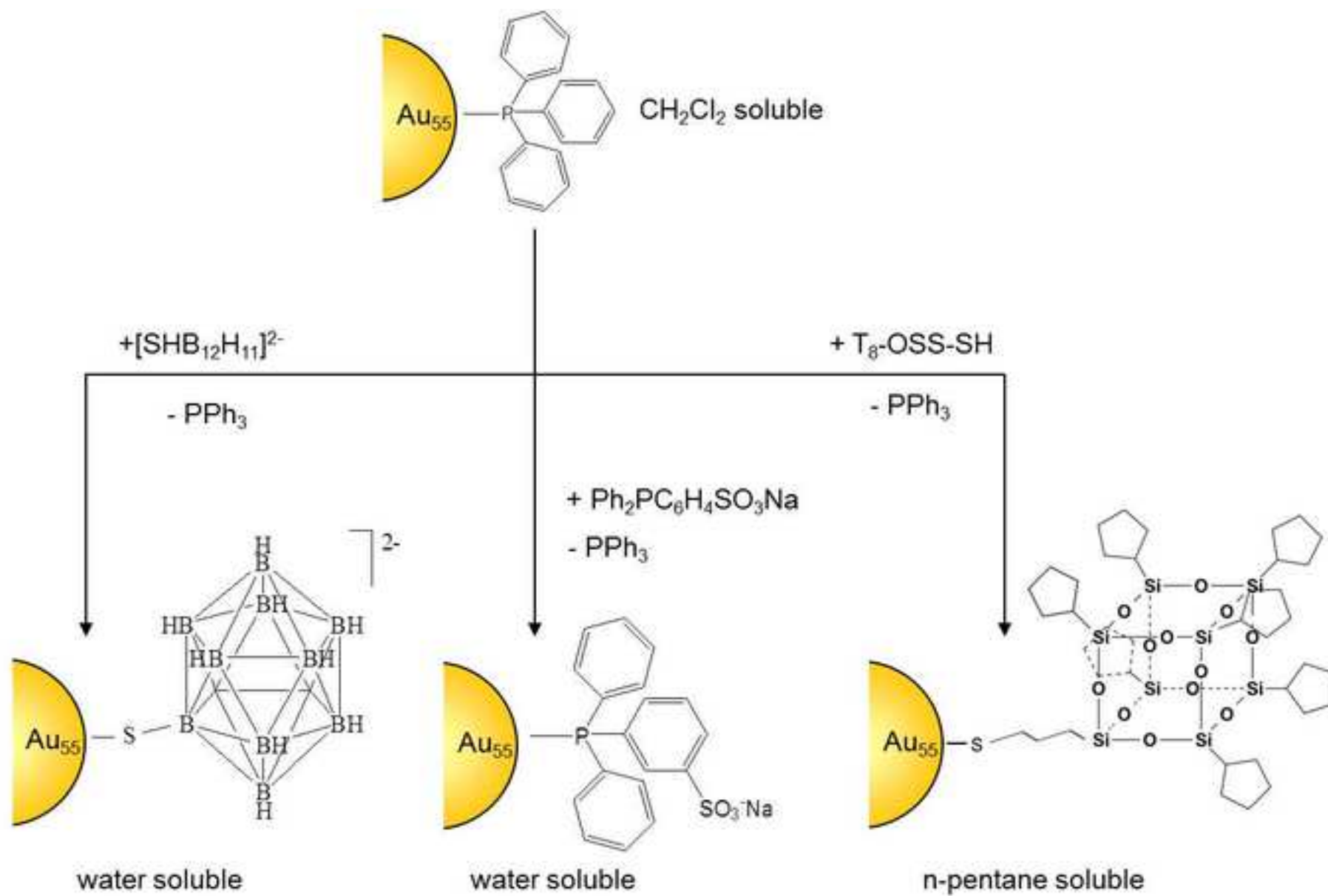
A) Minimum inhibitory concentration (MIC) in $\times 10^{-6}$ m				
	<i>E. coli</i>	<i>S. aureus</i>	<i>S. epidermidis</i>	<i>P. aeruginosa</i>
Au0.8MS	No inhibition	25	25	No inhibition
Au1.4MS	No inhibition	25	25	≥ 400
Au5.1MS	≥ 400	≥ 400	≥ 400	≥ 400
Au8.7MS	≥ 400	≥ 400	≥ 400	No inhibition
Au10.4MS	≥ 400	≥ 400	≥ 400	No inhibition
AuroVist	No inhibition	No inhibition	No inhibition	≥ 400

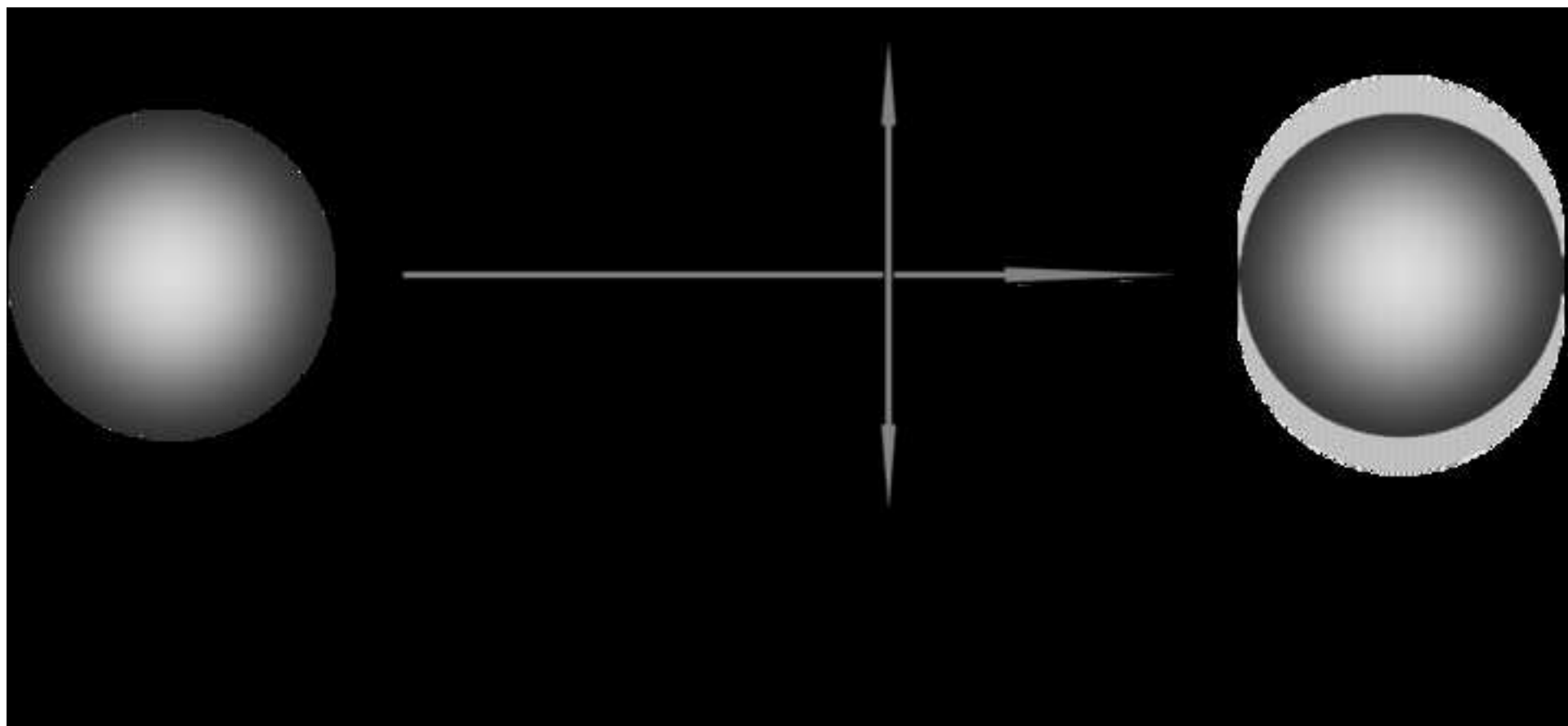
(B) Minimum bactericidal concentration (MBC) in $\times 10^{-6}$ m				
	<i>E. coli</i>	<i>S. aureus</i>	<i>S. epidermidis</i>	<i>P. aeruginosa</i>
Au0.8MS	ND	25	25	ND
Au1.4MS	ND	25	25	ND

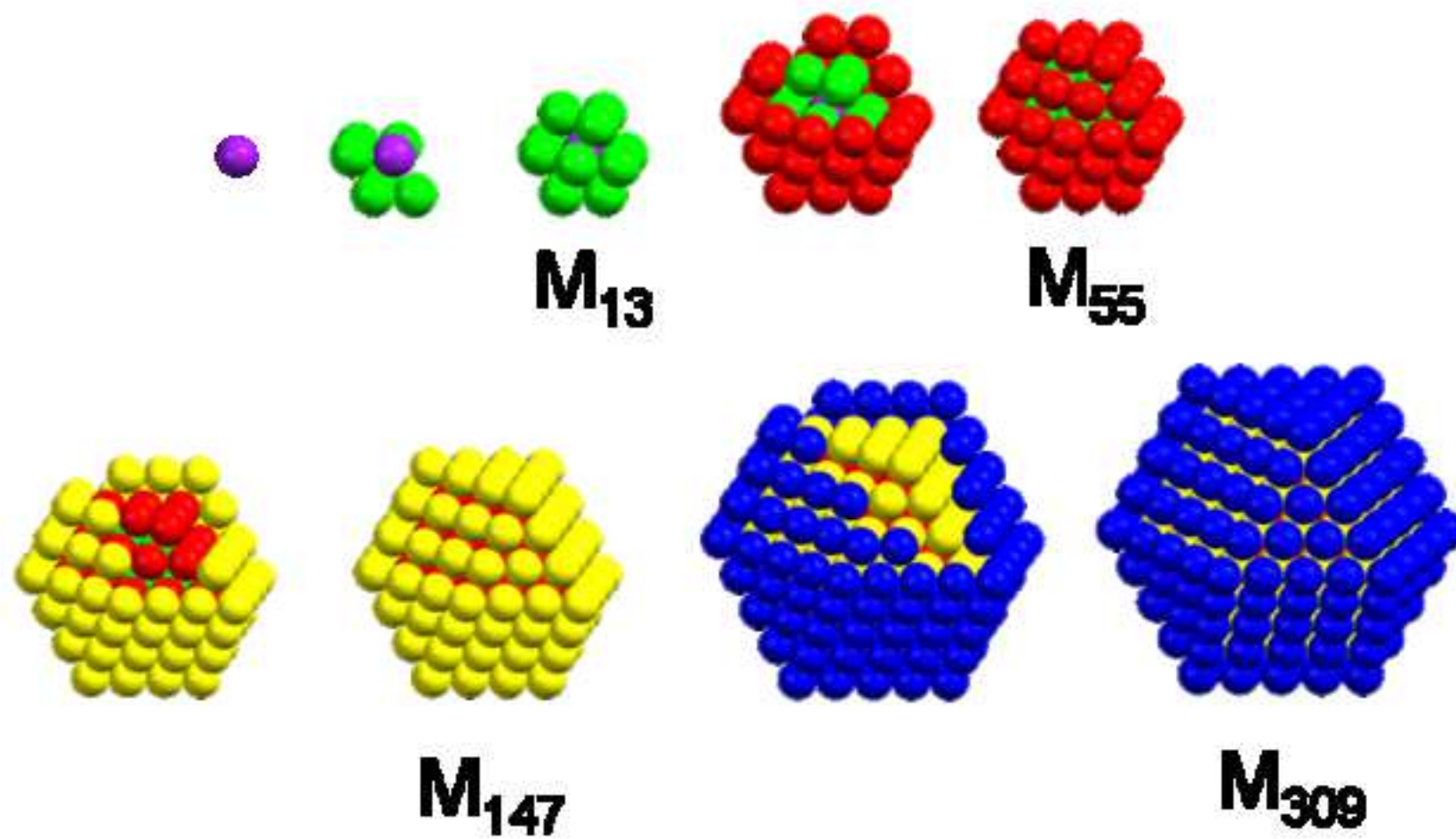
Note: The MIC and MBC values denoted above correspond to a minimum of four concordant experimental values obtained among 4–6 replicates. ND: not determined.

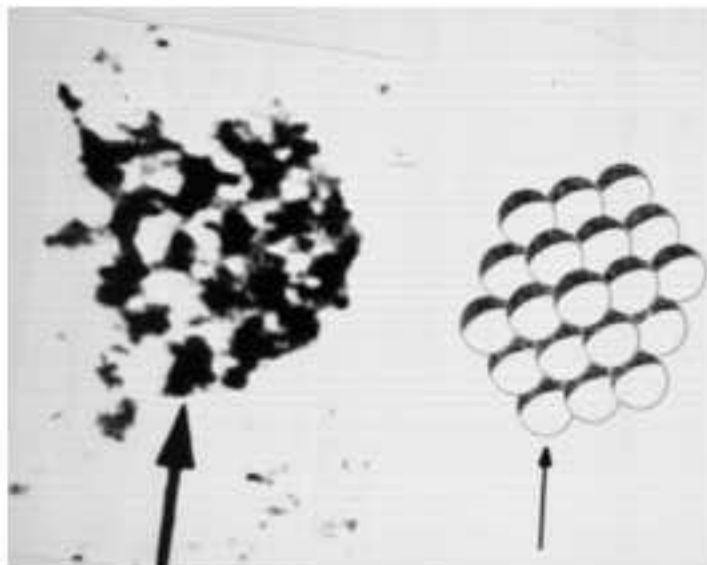
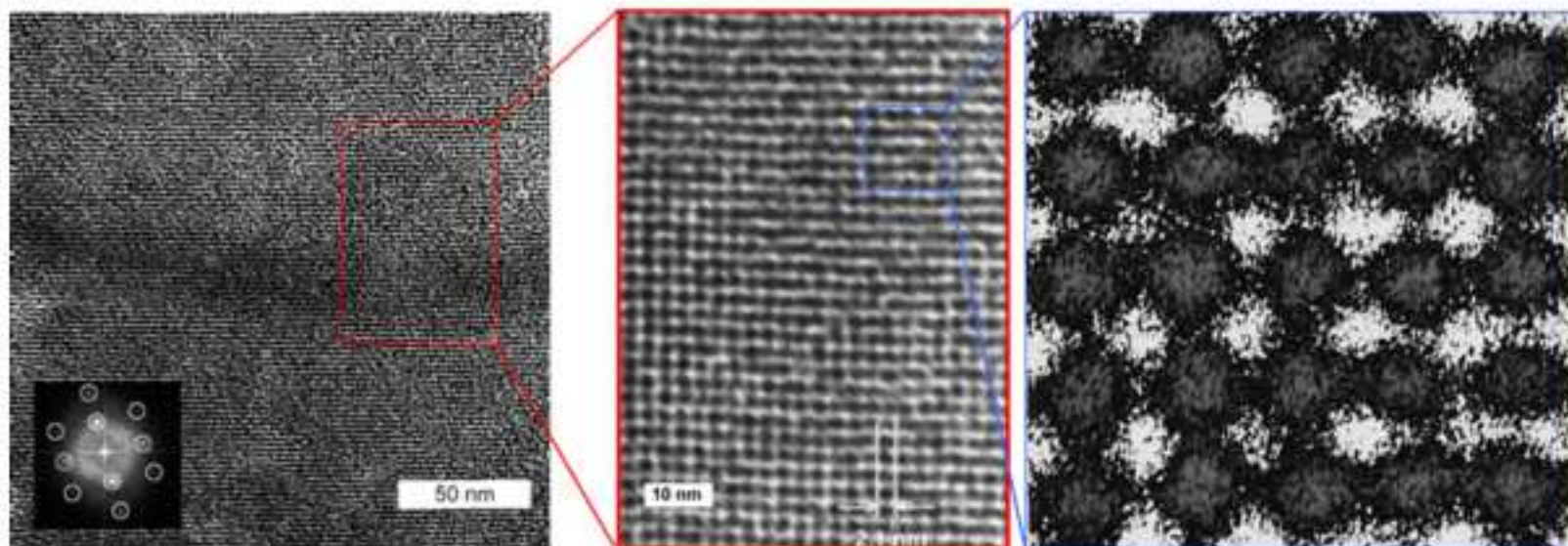


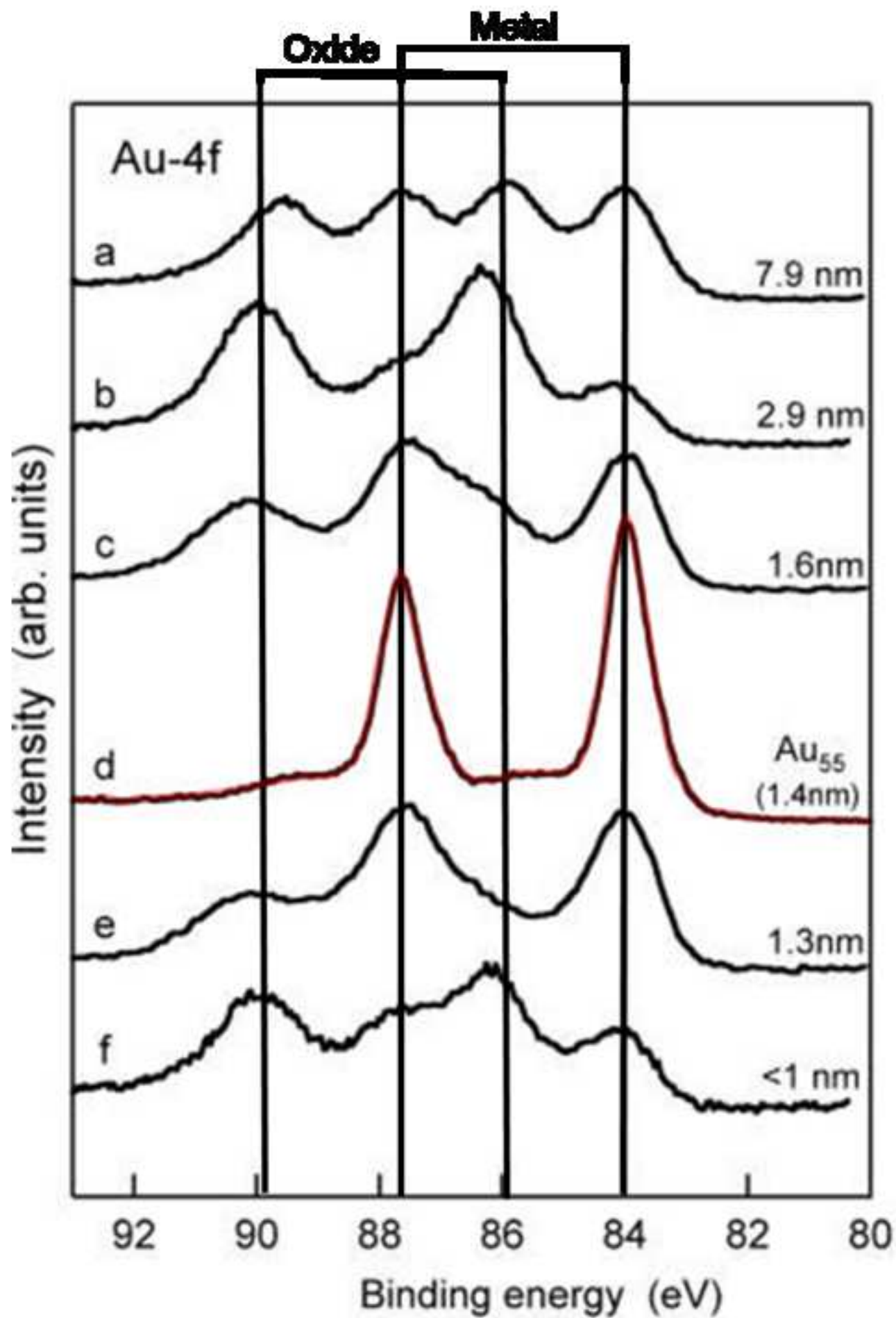


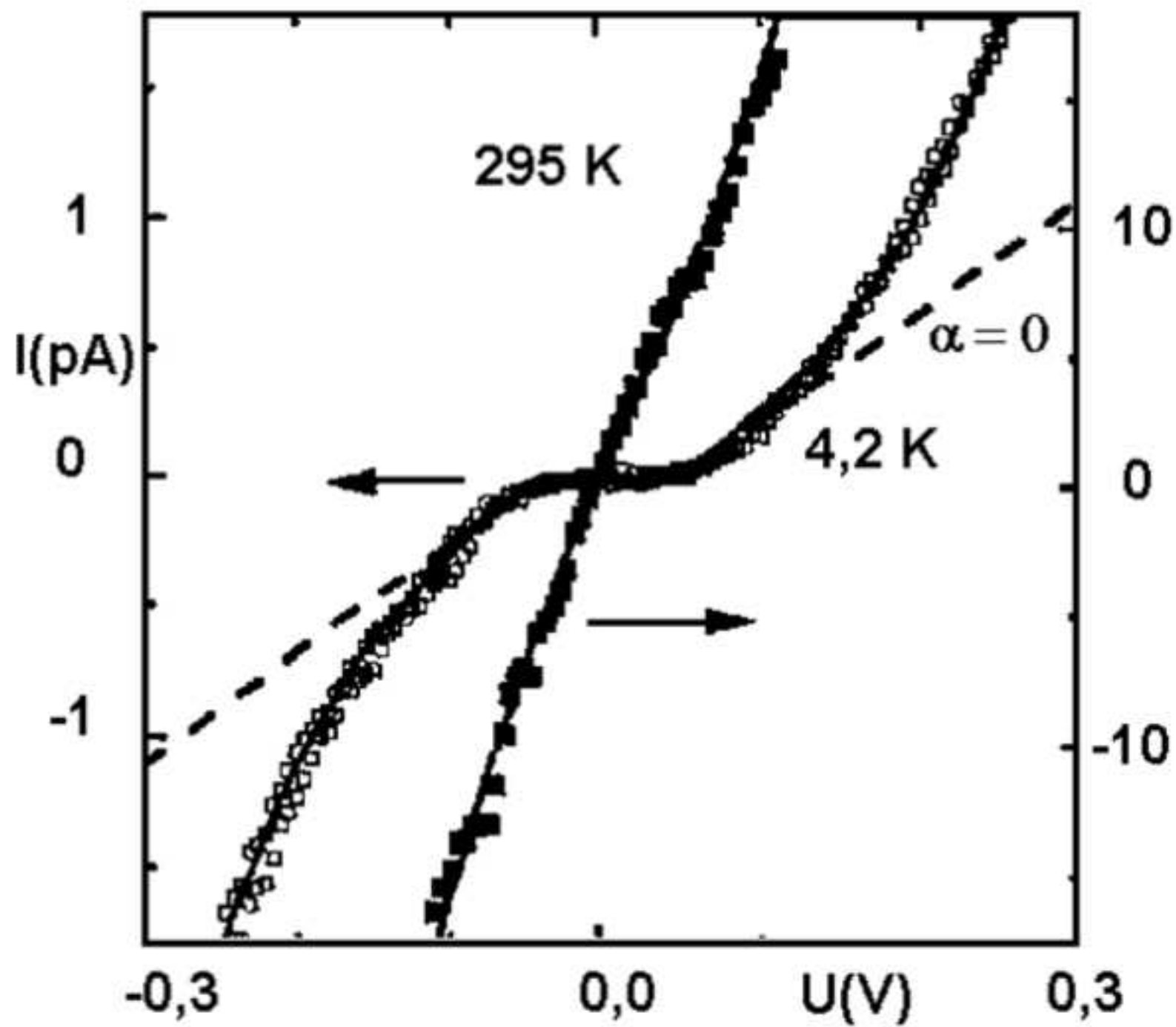


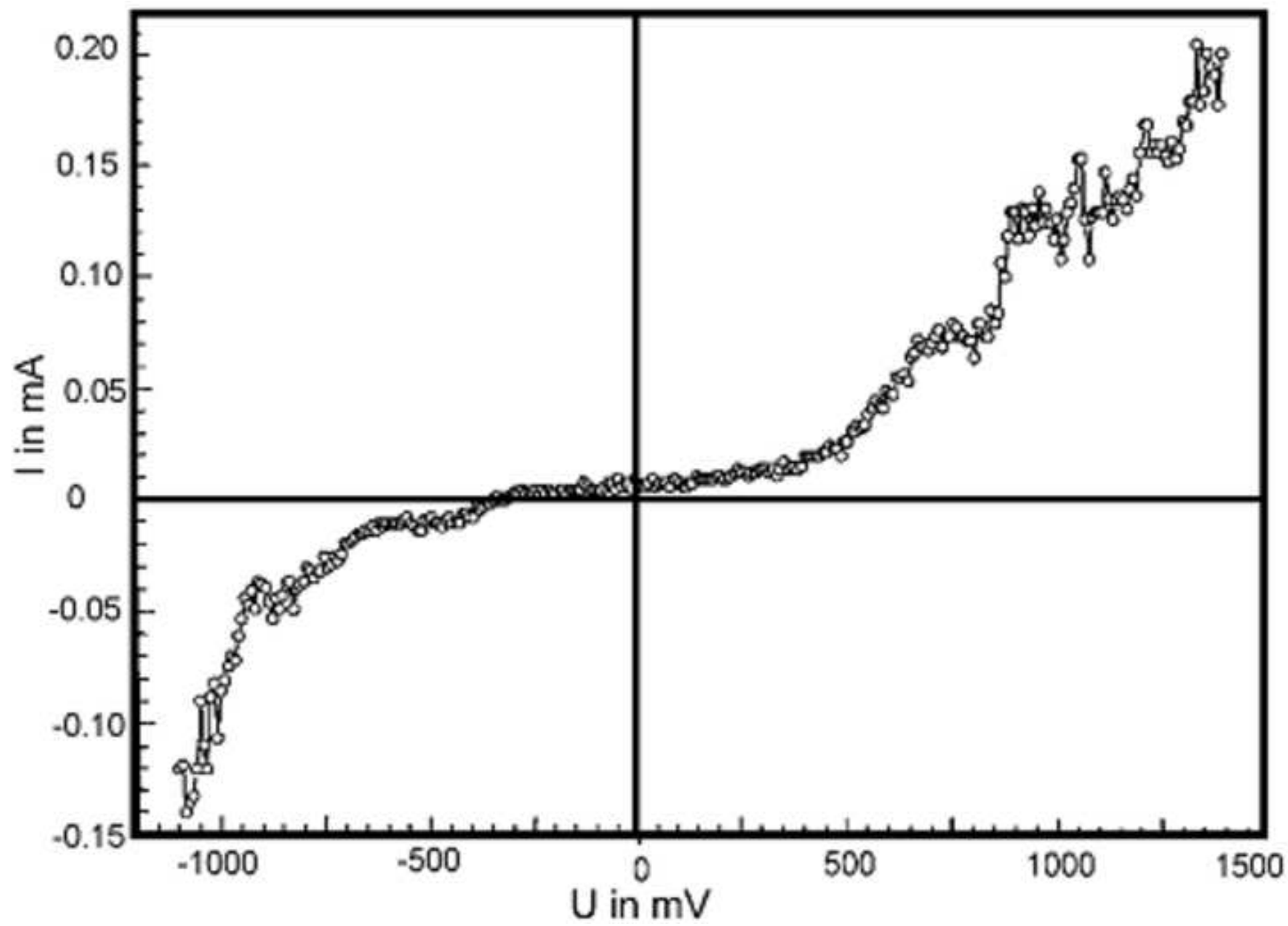


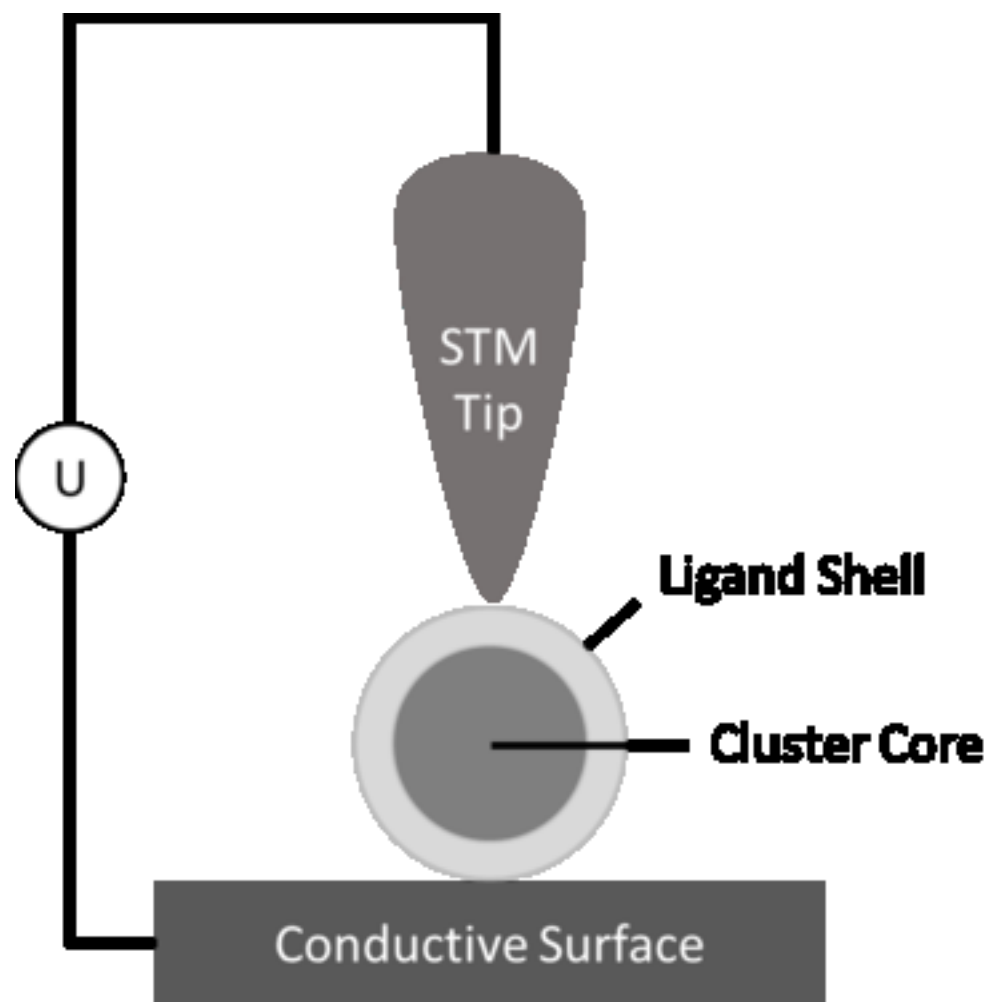


a)**b)**









$$\frac{e^2}{2C} \gg k_B T$$

C = Capacity of the tunnel contact

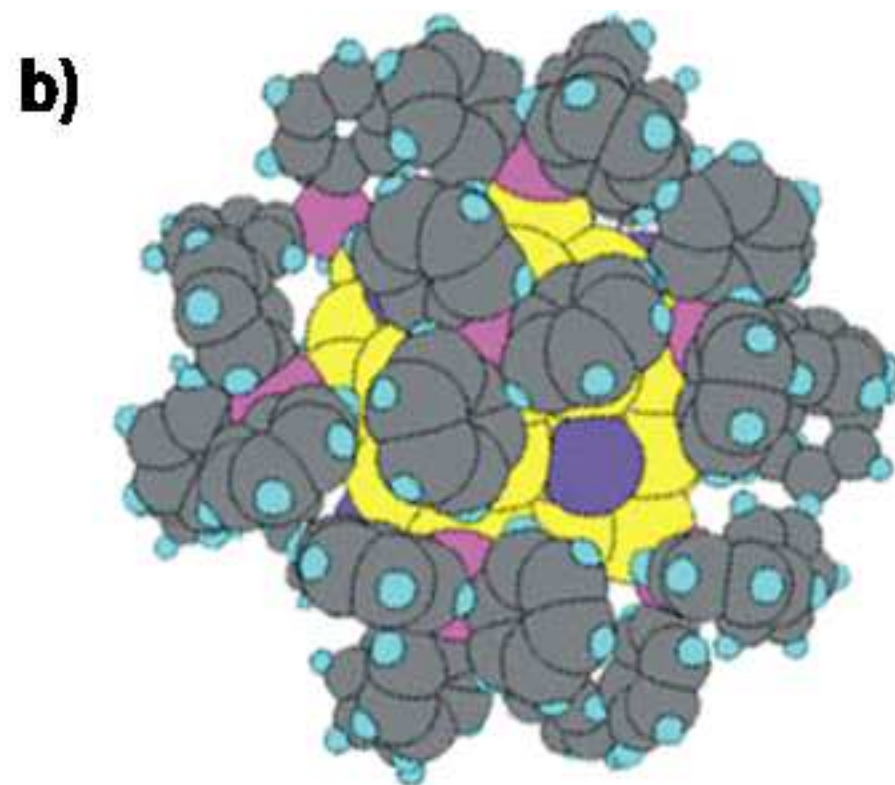
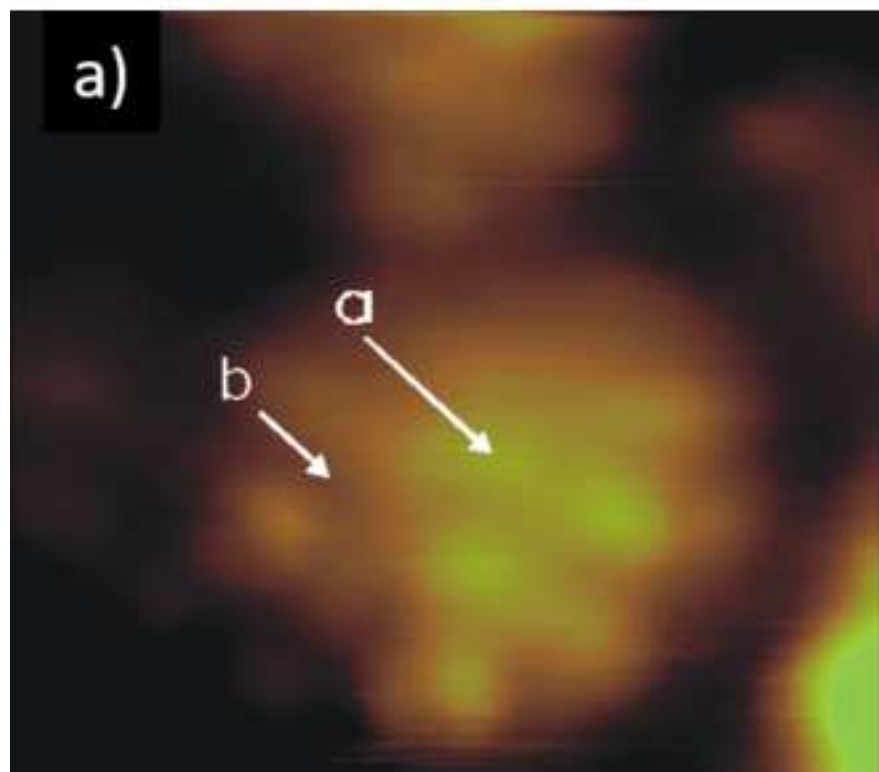
$$C = \epsilon \epsilon_0 \frac{A}{d}$$

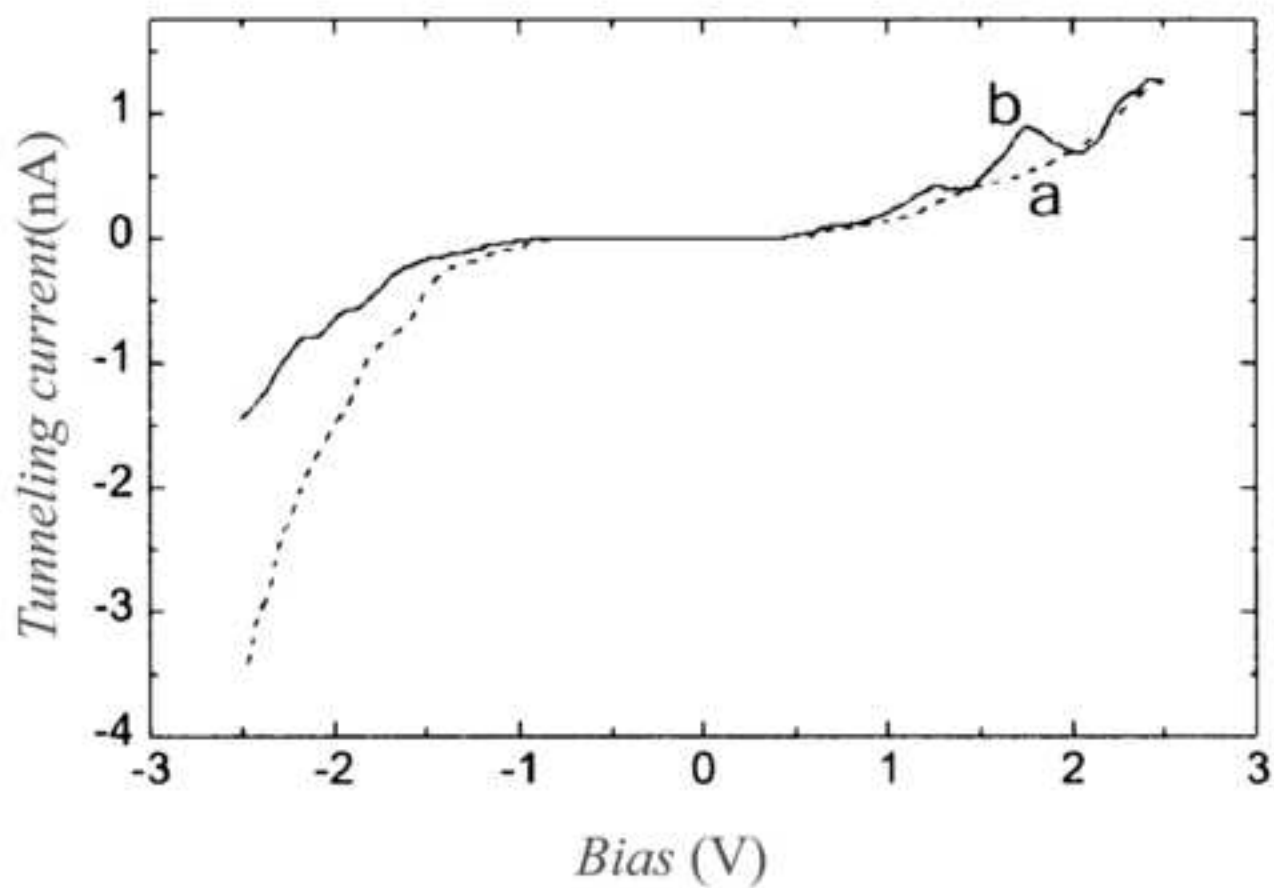
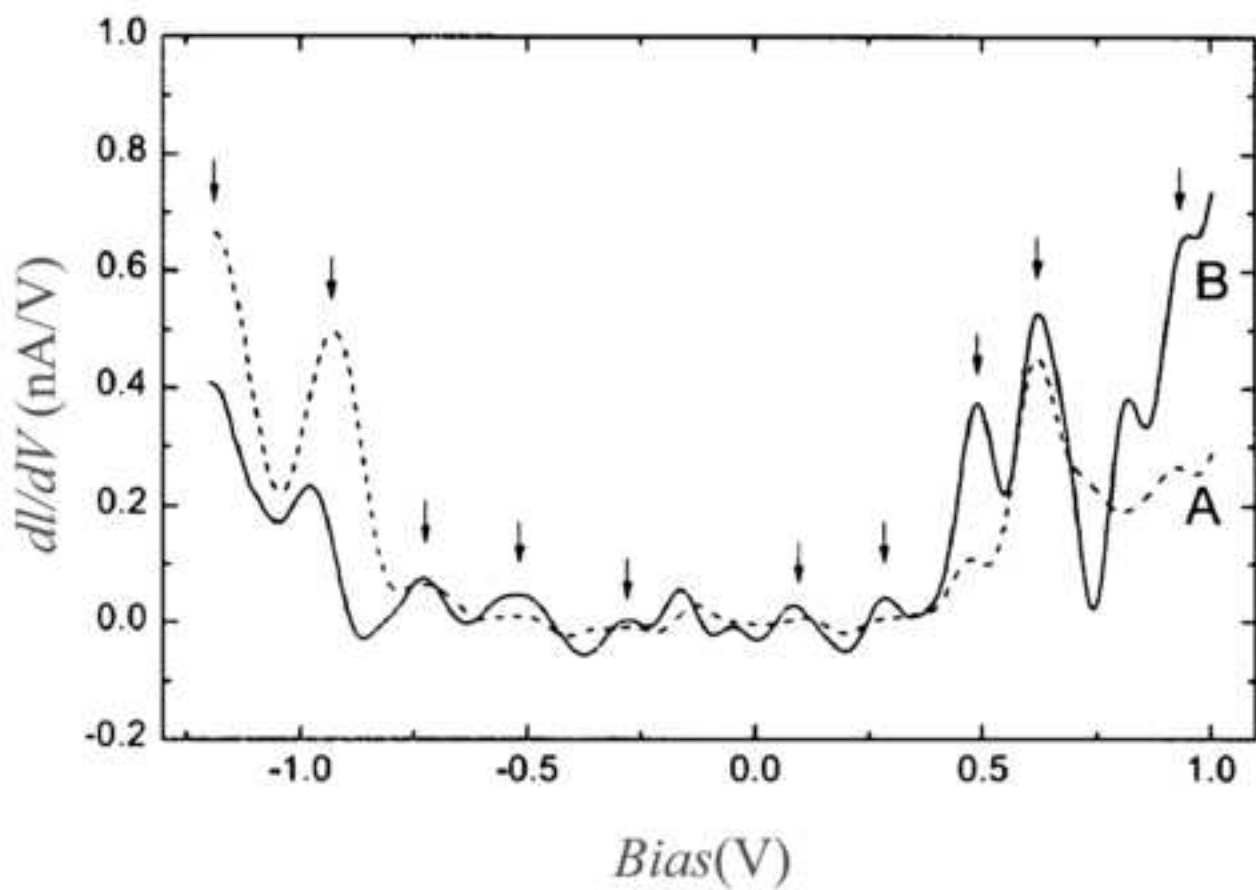
ϵ = dielectric constant

ϵ_0 = electric field constant

A = surface of the electrode

d = distance of the electrodes



**A****B**

